M.Sc. Thesis
Geophysics

Air-sea exchange of carbon dioxide at the island of Utö in the Baltic Sea

Martti Honkanen

2017

Supervisors:
Doc. Lauri Laakso and M.Sc. (Tech.) Juha-Pekka Tuovinen
Reviewers:
Prof. Timo Vesala and Doc. Lauri Laakso

UNIVERSITY OF HELSINKI
DEPARTMENT OF PHYSICS

PL 64 (Gustaf Hällströmin katu 2)
00014 Helsingin yliopisto

HELSINGIN YLIOPISTO – HELSINGFORS UNIVERSITET – UNIVERSITY OF HELSINKI

Tiedekunta/Osasto – Fakultet/Sektion – Faculty/Section Matemaattis-luonnontieteellinen	Laitos – Institution – Department Fysiikan laitos

Tekijä – Författare – Author
Martti Honkanen

Työn nimi – Arbetets titel – Title
Meren ja ilmakehän välinen hiilidioksidivaihto Utön saarella Itämerellä

Oppiaine – Läroämne – Subject
Geofysiikka

Työn laji – Arbetets art – Level Pro Gradu -tutkielma	Aika – Datum – Month and year Toukokuu 2017	Sivumäärä – Sidoantal – Number of pages 53

Tiivistelmä – Referat – Abstract

Hiilidioksidi on tärkeä yhdiste sekä ilmastonmuutoksen että meren perustuotannon kannalta. Valtamerien ja ilmakehän välistä hiilidioksidinvaihtoa ohjaa suurimittaiset virtaukset ja liukoisuuden muutokset, kun taas rannikkomerillä, kuten Itämerellä, hiilen kiertokulkuun vaikuttaa merkittävästi biologinen aktiivisuus. Meren ja ilmakehän välisen hiilidioksidivuon mittaaminen on kuitenkin haastavaa johtuen vuon pienuudesta, aalloista, jäästä ja vesiroiskeista. Pyörrekovarianssimenetelmä on laajalti käytetty menetelmä hiilidioksidivuon mittaamiseeen. Meren ja ilmakehän välistä hiilidioksidivuota usein lasketaan myös käyttäen tuulennopeuteen perustuvaa parametrisaatiota.

Ilmatieteen laitos ja Suomen ympäristökeskus aloittivat uuden merentutkimusaseman rakentamisen Utön saarelle Saaristomerelle vuonna 2012. Tämän tutkimuksen tavoitteena on määrittää aseman laitteiston soveltuvuus hiilidioksidivuomittauksiin ja vedenalaisen karbonaattijärjestelmän tutkimiseen. Meren ja ilmakehän välistä hiilidioksidivuota mitattiin loka-joulukuussa 2016 kolmella infrapunakaasuanalysaattorilla, minkä lisäksi vuo laskettiin käyttämällä parametrisaatiota kaasunvaihtokertoimelle. Pintaveden karbonaattijärjestelmää heinä-lokakuussa 2016 tutkittiin mittaamalla liuennutta hiilidioksidikonsentraatiota ja pH:ta läpivirtauslaitteistossa. Liuenneen hiilidioksidin konsentraatio mitattiin käyttämällä tasapainotuskammiota ja infrapunakaasuanalysaattoria.

Rannalle pystytetyllä vuomastolla voidaan mitata ilmakehän ja meren välistä hiilidioksidivuota käyttämällä avomerta vastaavia tuulensuuntia, jotka tässä tutkielmassa määritettiin pinnan rosoisuuden mukaan. Suljettu kaasuanalysaattori (Licor LI-7000) toimii haastavissa rannikko-olosuhteissa, kun taas avonaisella kaasuanalysaattorilla (Licor LI-7500) oli vaikeuksia toimia sateen ja korkean suhteellisen kosteuden aikana. Pearsonin korrelaatiokerroin kahden suljetun kaasuanalysaattorin välillä oli 0.91. Parametrisaatiolla laskettu vuo korreloi vain heikosti mitattujen voiden kanssa korrelaatiokertoimen ollessa 0.13. Läpivirtauslaitteistolla voidaan mitata vedenalaisen epäorgaanisen hiilen järjestelmää. Mitattu pH ja liuennut hiilidioksikonsentraatio olivat yhteydessä toisiinsa. Lisäksi osoittautui, että LI-7000 on herkkä mittalaitteen sisäisen lämpötilan muutoksille.

Avainsanat – Nyckelord – Keywords
Hiilidioksidi, liuennut hiilidioksidi, Itämeri, Ilma-meri kaasunvaihto, Pyörrekovarianssimenetelmä

Säilytyspaikka – Förvaringställe – Where deposited
Kumpulan kampuskirjasto

Muita tietoja – Övriga uppgifter – Additional information

HELSINGIN YLIOPISTO – HELSINGFORS UNIVERSITET – UNIVERSITY OF HELSINKI

Tiedekunta/Osasto – Fakultet/Sektion – Faculty/Section Faculty of Science	Laitos – Institution – Department Department of Physics

Tekijä – Författare – Author
Martti Honkanen

Työn nimi – Arbetets titel – Title
Air-sea exchange of carbon dioxide at the island of Utö in the Baltic Sea

Oppiaine – Läroämne – Subject
Geophysics

Työn laji – Arbetets art – Level M. Sc. Thesis	Aika – Datum – Month and year May 2017	Sivumäärä – Sidoantal – Number of pages 53

Tiivistelmä – Referat – Abstract

Carbon dioxide is a key compound both in climate change and marine biological productivity. In the oceans, the sea-air exchange of carbon dioxide is driven by large-scale currents and changes in solubility, whereas in coastal seas, such as the Baltic Sea, biological activity has a significant effect on the aquatic carbonate system. However, direct measurements of the sea-air exchange of carbon dioxide are difficult to carry out due to the small magnitude of the fluxes, waves, sea ice and sea spray that influence sensitive instruments. Eddy covariance method is a widely used direct method for measuring the fluxes of carbon dioxide. The sea-air fluxes of carbon dioxide are also commonly calculated using a parametrization based on wind speed.

Finnish Marine Institute in collaboration with Finnish Environment Institute began to construct a new atmospheric and marine research station on Utö in the Archipelago Sea in 2012. The objective of this study is to determine the suitability of the new station to measure air-sea exchange of carbon dioxide and aquatic carbonate system. The air-sea fluxes of carbon dioxide were measured with three infrared gas analyzer set-ups during October-December 2016, and the fluxes were also calculated using a parametrization of gas transfer velocity. The aquatic carbonate system of the surface water during July-October 2016 was studied using dissolved carbon dioxide concentration and pH of the seawater measured in a flow-through pumping system. The dissolved carbon dioxide concentration was measured by using an equilibration chamber together with an infrared gas analyzer.

The micrometeorological tower erected on the shore can be applied for measuring the sea-air fluxes of carbon dioxide in an open sea wind sector, which was determined based on the roughness length. The closed-path infrared gas analyzer (Licor LI-7000) works well in the hard coastal conditions, whereas an open-path analyzer (Licor LI-7500) had difficulties in measuring fluxes during showers and high relative humidity. The Pearson correlation coefficient between the fluxes measured with two closed-path gas analyzer set-ups was 0.91. The flux calculated using a parametrization of gas transfer velocity showed only a small correlation with the measured flux, with a Pearson correlation coefficient of 0.13. The flow-through pumping system can be used to calculate the components of the aquatic inorganic carbonate system. The measured pH was linked to the dissolved carbon dioxide concentration of the sea water. Additionally, it was discovered that the LI-7000 is sensitive to changes in instrument temperature.

Avainsanat – Nyckelord – Keywords
Carbon dioxide, dissolved carbon dioxide, Baltic Sea, air-sea exchange, Eddy Covariance method

Säilytyspaikka – Förvaringställe – Where deposited
Kumpula Campus Library

Muita tietoja – Övriga uppgifter – Additional information

Contents

Symbols

C_a	Concentration in the air
C_0	Concentration at the surface of the water
C_w	Concentration in the bottom of water surface layer
Co_{wC}	Cospectrum of vertical velocity and CO_2 mixing ratio
Co_{wT}	Cospectrum of vertical velocity and air temperature
c_p	Specific heat capacity of air
D	Molecular diffusivity
F_{CO_2}	Carbon dioxide flux
f	Frequency
g	Gravitational acceleration
h	Measurement height
H	Sensible heat flux
K_0	Aqueous-phase solubility
K_1	1st dissociation constant of carbonic acid
K_2	2nd dissociation constant of carbonic acid
K_w	Equilibrium constant of water
k	Gas transfer velocity
L	Obukhov length
n	Normalized frequency
p	Partial pressure
pCO_{2a}	Partial pressure of CO_2 in air
pCO_{2w}	Partial pressure of CO_2 in water
S	Sink/source strength
Sc	Schmidt number of CO_2
TA	Total concentration of inorganic carbon

TIC	Total inorganic carbon
T_a	Air temperature
T_i	Instrument temperature
T_{wC}	Transfer function of vertical velocity and CO_2 mixing ratio
t	Time
u	Wind velocity
U	Wind speed
U_8	Wind speed at the height of 8 m
U_{10}	Wind speed at the height of 10 m
u_*	Friction velocity
w	Vertical velocity
z	Height
z_0	Surface roughness
ϵ	Molar fraction error
δ	Layer thickness
κ	von Karman constant
σ_w	Standard deviation of vertical velocity
ρ_a	Density of air
ρ_d	Density of dry air
τ	Surface stress
Θ_v	Virtual potential temperature
ζ	Arbitrary atmospheric quantity
χ	Mixing ratio
ξ	Stability parameter

1 Introduction

Carbon dioxide (CO_2), next to water vapour, is the most important greenhouse gas. Anthropogenic actions, such as combustion of fossil fuels and land use changes, have caused a significant increment in concentration of CO_2 since the industrial revolution(Etheridge et al. 1996). To model the future climate one must understand the present carbon cycle.

Carbon dioxide has a fundamental impact on the pH of the oceans. The oceans have become more acidic due to the excess amount of CO_2. The acidification of seas has raised concerns about the adaptation of marine ecosystems to lower pH since the sedimentation of calcium carbonate is a function of pH. Climate change will also lower the pH of the Baltic Sea(Omstedt et al. 2012).

CO_2 is exchanged between terrestrial biosphere, atmosphere and oceans rapidly(Falkowski et al. 2000). In the atmosphere, carbon exists mostly in the forms of carbon dioxide and methane. Methane, however, is much less abundant than CO_2. Carbon dioxide is exchanged between the biospheric and atmospheric pools through respiration and photosynthesis. It also can dissolve into water and can be removed from terrestrial biosphere by combustion. Generally, the oceans act as sinks and bind up to 25% of anthropogenic CO_2 emissions to atmosphere(Heinze et al. 2015). On a global scale, the transport of aquatic CO_2 is governed by large-scale ocean circulation. As the water gets cooler at high latitudes, the solubility of CO_2 increases. CO_2 is transported to the deep water in the North Atlantic Ocean and the Southern Ocean(Falkowski et al. 2000).

The sea-air CO_2 exchange of the Baltic Sea differs from that of oceans in biological activity as photosynthesis binds the atmospheric CO_2. Of all ocean area, 7% is located on the continental shelves. Inspite of their small area, coastal seas are responsible of 15–30% of all primary production(Kulinski and Pempkowiak 2011). This is due to the biological activity that is driven by nutrient-rich river flows. Also, one special feature of the Baltic Sea that affects the air-sea gas transfer is that it has an ice cover for 5–7 months a year(Myrberg et al. 2006, p.31).

Atmospheric CO_2 concentration variations through the Baltic Sea have been studied by Rutgersson et al. (2009) using data consisting of measurements from inland sites, ships and an island. Using the same measurement sites as Rutgersson et al. (2009) did, Norman (2013) studied the air-sea fluxes of CO_2 in the Baltic Sea. Thomas and Schneider (1999) studied the seasonality of CO_2 in the Baltic Sea using ship measurements. Kulinski and Pempkowiak (2011) calculated the carbon budget of Baltic Sea using a mass balance approach, and Omstedt et al. (2009) modelled the uptake and release of CO_2 in the Baltic Sea. The spatial, and temporal in the case of cruises, resolution of CO_2 measurements in the Baltic Sea is low, and little attention has been paid to the Archipelago Sea.

To gain better understanding of the variability of CO_2 fluxes through the Baltic Sea and aquatic carbonate system of the Baltic Sea, the Finnish Meteorological Institute in collaboration with the Finnish Environment Institute began to construct a new atmospheric and marine research station on Utö in the Archipelago Sea in 2012. Also, it will provide information about the connection between the ecosystem functioning and environmental variables. A micrometeorological measurement tower is set up on the shore to measure CO_2 and energy fluxes. A flow-through pumping system was installed for measuring physical, chemical and biological properties of seawater, including dissolved CO_2 concentration.

The results from this station are examined in this thesis. The main objective of this thesis is to determine suitability of the new setup to monitor the marine CO_2 system. We wanted to find out if we can measure the sea-air fluxes of CO_2 with the flux tower positioned on an island. In particular, we focused on the technical solutions needed to perform long-term measurements in harsh coastal conditions. Also, we wanted to see if the flow-through pumping system can improve our understanding of the aquatic carbonate system. First, the pools of carbon dioxide are briefly discussed, while special attention is paid to the aquatic carbonate system and the Baltic Sea. Next, the air-sea interface and the gas exchange are presented. The method for measuring the gas exchange, eddy covariance method, is introduced. The air-sea fluxes of CO_2 measured with three infrared gas analyzer set-ups and the flux calculated using a parametrization of gas transfer velocity during 14 October 2016 – 14 December 2016 are compared. This includes a brief spectral analysis for determining the frequency responses of the analyzers. Also, aquatic inorganic carbon system of the surface water during 5 July – 3 October 2016 is studied.

2 Theory

2.1 Carbon in the ecosystems

Due to their electrical neutrality, carbon atoms easily bind with other carbon atoms and other atoms, creating stable compounds. This makes carbon vital for all lifeforms. In the atmosphere, the most common carbon compounds are carbon dioxide (CO_2), methane (CH_4) and unstable carbon monoxide (CO), which oxidizes to carbon dioxide.

Carbon dioxide is the building material for the living organisms. Through photosynthesis, plants transform CO_2 and H_2O to carbohydrates. This process is controlled by the amount of light, but also the availability of nutrients, mainly nitrate and phosphorus, plays an important role. CO_2 returns to the atmosphere through cellular respiration and wildfires.

2.1.1 Aquatic inorganic carbon system

Since the oceans cover over two-thirds of the planet's surface, it is not a surprise that a roughly half of the primary production takes place in the oceans(Beer et al. 2014, p. 2). In the mid-latitudes the growth of biomass occurs in the spring and decrease in the summer. By the end of the summer, phytoplankton dies as the availability of nutrients decreases while the stratification blocks more nutrients coming from deep water. In the autumn, the stratification breaks down and a new growth of biomass may appear.

Carbon dioxide dissolves into water. The solubility decreases with increasing water temperature. Further, the dissolved carbon dioxide together with water forms carbonic acid: $CO_2\,(aq) + H_2O\,(l) \longleftrightarrow H_2CO_3\,(aq)$. Next, the carbonic acid dissosiates into bicarbonate ion: $H_2CO_3 \longleftrightarrow {HCO_3}^- + H^+$. As much as 95% of the inorganic carbon in the oceans is in the form of bicarbonate ion(Kagan 1995). Bicarbonate ion dissosiates further into a carbonate ion: ${HCO_3}^- \longleftrightarrow {CO_3}^{2-} + H^+$. The concentration of carbonate ions grows until the solubility limit of calcium carbonate has been reached: $CaCO_3 \longleftrightarrow Ca^{2+} + {CO_3}^{2-}$. The calcium carbonate exists in two different crystal forms: calcite and aragonite. The addition of cations by slow weathering of rocks buffer the changes in CO_2 concentration(Falkowski et al. 2000).

Generally speaking, the oceans are carbon sinks but there are spatial differences. The equator is a source because upwelling rises carbon rich water to the surface and carbon dioxide dissolves poorly in high temperatures. Wanninkhof et al. (2009) notes that the gas exchange between the air and the sea alleviates the global greenhouse effect by binding part of the excessive carbon dioxide in the oceans.

The inorganic carbon consists of carbon dioxide, bicarbonate ion and carbonate ion, so the total concentration of inorganic carbon is $TIC = [CO_2] + [{HCO_3}^-] + [{CO_3}^{2-}]$. TIC increases when moving further away from the equator. In the surface layer, the amount of inorganic carbon is naturally reduced by photosynthetic activity of phytoplankton. Because the phyto- and zooplankton fall to the deep water and decompose there, TIC increases with the depth. Falkowski et al. (2000) note that a quarter of the carbon in the surface water will sink into the deep water.

The binding of anthropogenic CO_2 causes the acidification of the oceans(Feely et al. 2009). As already mentioned, when carbonic acid dissociates, it also releases hydgrogen ions and thus lowers the pH of water. However, the pH balance in seawater is also controlled by the total alkalinity, TA, which is determined as the excess of the proton acceptors over the amount of proton donors. The most important proton acceptors are bicarbonate, carbonate and borate ions, and the most important pro-

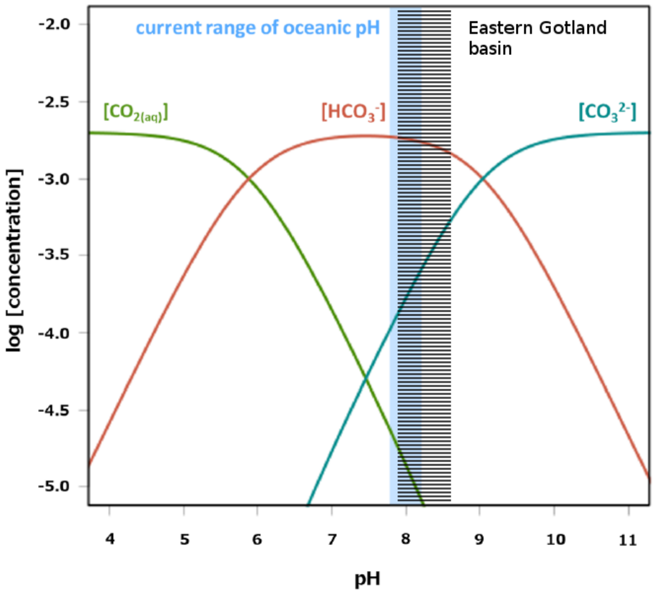

Figure 1: The dominant inorganic carbon species as a function of pH(Heinze et al. 2015). Modified: Added pH range of Eastern Gotland Basin in 1993–2008(Omstedt et al. 2010). The concentration is expressed in units of $\mathrm{mol\,l^{-1}}$.

ton donors are hydrogen ions and hydrogen sulphate ion(Omstedt et al. 2010). The lowered pH reduces the concentration of calcium carbonate, and therefore it is harmful for the formation of corals. Fig. 1 shows the so-called Bjerrum plot, which depicts the concentration of different inorganic carbon compounds as a function of pH when the compounds are in equilibrium. For typical pH of oceans, the dominant compound is bicarbonate. Bicarbonate is also the dominant species in the Baltic Sea but the proportion of carbonate ions is higher than in the oceans and the proportion of carbon dioxide, on the other hand, is lower than in the oceans.

2.2 The Baltic Sea

The Baltic Sea is a shallow mediterranean sea of the Atlantic ocean, meaning that the Baltic Sea is a semi-closed sea with a limited exchange of water with the Atlantic Ocean. A mean depth is 54 m and the deepest place is Landsort Deep with a depth of 459 m(Myrberg et al. 2006, p. 18). The only connection to the Atlantic Ocean is through the shallow and narrow straits of Denmark, the 8 m deep Drogden Sill and the 18 m deep Dars Sill, where saline water flows into the Baltic Sea. Nutrient-rich fresh water flows in from the rivers from the nine countries that border the Baltic sea, which reflects on the nutrient load. Most of the river inflow takes place in northern parts of the the Baltic Sea: the Bay of Bothnia, the Bothnian Sea and the Gulf of Finland receive about two-thirds of total river runoff(Myrberg et al. 2006, p. 93). This causes the water to be brackish, and there is a clear salinity gradient: the salinity decreases from about $30\,\mathrm{gkg}^{-1}$ in the straits of Denmark to about $0\,\mathrm{gkg}^{-1}$ in the northeast(Myrberg et al. 2006, p. 18). Water is also stratified, causing hypoxia in the deep parts of the Baltic Sea.

In the spring, after the solar radiation has melted the ice cover, the surface water will reach the temperature of maximum density, which will start the mixing of the water column. As the temperature keeps rising a stable surface layer will develop. Under this layer, there is a thermocline, where the vertical temperature profile undergoes a significant change, and the deep water. The thermocline restricts vertical mixing so the algae do not get the replenishment of nutrients from the deep water. In the autumn, the surface water cools and the second vertical mixing occurs.

During the winter the Baltic Sea freezes, at least partially. The largest annual ice coverage is 45% on average(Myrberg et al. 2006, p.139) and the ice is present for 5–7 months a year(Myrberg et al. 2006, p.31). The fast ice will be located on coasts, and on open sea one can encounter drift ice.

The atmosphere above the Baltic Sea has its carbon dioxide concentration maximum during the winter and the minimum concentration is measured in summer (Fig. 2). The timings of maximum and the minimum concentrations are delayed when moving towards the North(Rutgersson et al. 2009).

The dissolved carbon dioxide in the surface water is controlled by sea-air gas exchange, biological activity and mixing. During the summer,

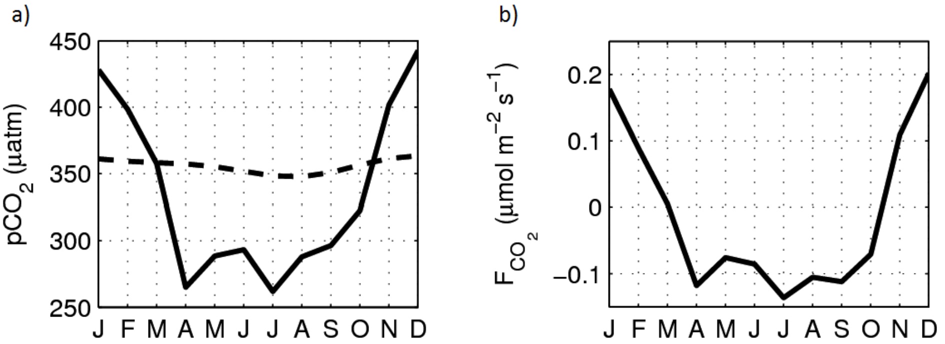

Figure 2: Modelled monthly average of a) atmospheric carbon dioxide partial pressure (dashed line) and dissolved carbon dioxide partial pressure (solid line) and b) carbon dioxide fluxes in the Eastern Gotland basin(Norman 2013).

primary production consumes the CO_2, whereas in the winter mineralization and mixing increase the CO_2 levels in the surface water. Wesslander (2011) notes that during the winter the wind deepens the mixed surface layer to halocline, which brings CO_2-rich water to surface.

The difference between the CO_2 partial pressure in the atmosphere and surface water controls the air-sea flux of CO_2. During the winter, the surface waters of the Baltic Sea has on average a higher partial pressure of CO_2 than the atmosphere, and the sea acts as a source of CO_2. In the summer the sea is a sink. Löffler et al. (2011) emphasize that sea ice has a huge effect on gas exchange: during the winter the ice cover restricts the release of the carbon dioxide to air, and it also delays the spring bloom of phytoplankton.

The spatial differences in nutrient-rich riverine input make the Baltic Sea a diverse carbonate system. Biological activity is higher in the southern parts of the Baltic sea. The ratio of photosynthesis and respiration varies through the Baltic Sea resulting in a variation in the air-sea CO_2 exchange. The Gulf of Bothnia has a low primary production and thus it acts as an source of carbon dioxide, whereas the Baltic proper has a high primary production and constitutes an annual net sink(Kulinski and Pempkowiak 2011). In particular, Löffler et al. (2011) found out that the central parts of the Gulf of Bothnia acted as a sink, whereas shallow waters were sources. There is disagreement whether the Baltic Sea is a net sink or a source. Wesslander (2011) proposed that the Baltic Sea has an interannual variability in the net uptake and release of CO_2.

Geological properties in the drainage area affect the alkalinity. Due to weathered limestone, south-eastern parts of Baltic Sea have a higher buffering capacity than northern Baltic Sea(Wesslander 2011).

2.3 Atmospheric boundary layer

The lowest part of the atmosphere, extending to several tens of meters to several kilometers(Arya 2001, p.3), is called the boundary layer, BL (Fig. 3). Flow structure in the BL is influenced by surface friction and temperature gradient and also the earth's rotation(i.e. coriolis effect). Whereas flow in free atmosphere above BL is streamlined, i.e. laminar, the flow in the BL is more or less chaotic, i.e. turbulent. The turbulence enables efficient mixing of atmospheric quantities and exchange of them with the surface.

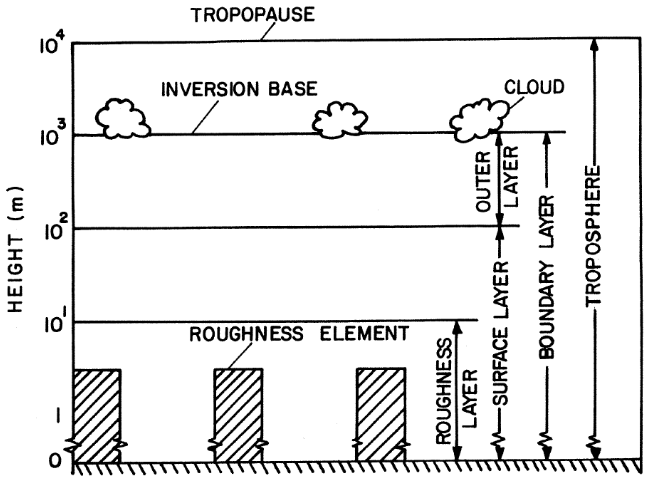

Figure 3: The structure of the troposphere(Arya 2001, p.2).

The height of the boundary layer changes depending on cooling and heating of the surface, wind speed and surface roughness. Due to the diurnal changes in radiative heating, the height of the BL can vary markedly during the day. However, the diurnal variation in the BL height is smaller over sea than over land due to the high heat capacity of water. Air masses advected from the land can have an effect on the structure of BL over sea. Over the sea, the BL is also influenced by the surface waves of water.

The surface layer is located at the bottom of the BL, typically covering the lowest one-tenth or so of the boundary layer(Arya 2001, p.4), where the coriolis effect is negligible, so the flow structure is only influenced by surface friction and temperature gradient. In this layer, the atmospheric properties experience strong vertical gradients, and thus exchange of momentum, heat and mass between the surface and atmosphere is significant. The fluxes are also approximately constant with height. At the bottom of surface layer locates roughness layer, where individual roughness elements directly influence the flow.

Due to the surface friction winds near the surface slow down, thus creating a velocity gradient between the bottom and top of BL, i.e. wind shear. By assuming fully turbulent and horizontally homogenous surface layer, the mean wind shear depends only on height, z, surface stress, τ and density of air, ρ_a. The only length scale is z and the only velocity scale can be formed from τ and ρ_a: $u_* = (\tau/\rho_a)^{1/2}$, which is called friction velocity and represents the velocity scale of turbulent flow. This leads to a logarithmic profile of horizontal velocity:

$$U = \frac{u_*}{\kappa} \ln(\frac{z}{z_0}) \tag{1}$$

where U is wind speed, z_0 is roughness length and k is von Karman's constant, which is a universal constant for all surfaces. Eq. (1) is only valid for the neutral stability. In the case of unneutral conditions, the equation can be corrected with an additional stability correction parameter.

Commonly, stratification is described by Obukhov length, L, which defines a height at which turbulence generated by buoyancy outweighs turbulence generated by wind shear:

$$L = -\frac{\rho_a c_p u_*^3 \Theta_v}{kgH}, \tag{2}$$

where Θ_v is virtual potential temperature, c_p is the specific heat capacity of air, g is gravitational acceleration and H is sensible heat flux. If L is negative, the atmospheric stratification is unstable and buoyant forces enhance mechanical turbulence. In the case of stable stratification, $L > 0$, turbulence is suppressed by temperature stratification. Strictly speaking, the above mentioned verbal definition of L is only valid during stable stratification, as during unstable stratification, no physical height can be found where the turbulent magnitudes of buoyancy and shear are equal. Another widely used variable is stability parameter, ξ, which is defined as a ratio of the height to the Obukhov length. Stability determines the scale of turbulence and the efficiency of eddy transport(Garbe et al. 2014). In the unstable BL, the atmospheric quantities are well-mixed and are nearly constant with height(Jacob 1999, p. 60).

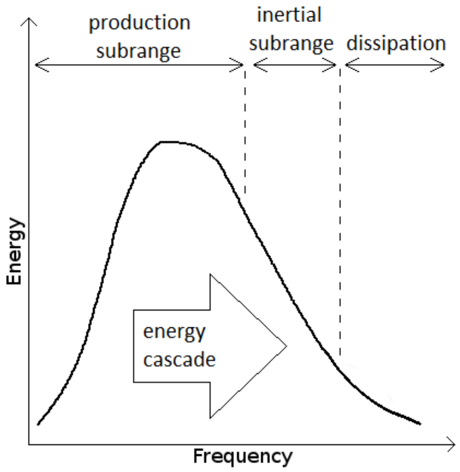

Figure 4: Schematic diagram of energy spectrum representing the turbulent energy as a function of frequency.

One way to think of turbulent flow is to consider it a supercomposition of eddies, or more commonly known as vortices, of different sizes(Burba and Anderson 2010). The the size of the smallest eddies are 1 mm and the largest are 10–500 m(Kaimal and Finnigan 1994, p. 35). The energy in turbulent flow is created by the shear and buoyancy forces. Larger eddies contain more kinetic energy and contribute to the transport of turbulence (Fig. 4). Due to the flow instabilities they break down to smaller eddies. This repeats itself until the eddies are so small that kinetic energy is transformed into thermal energy. Spectral analysis is a way to examine these energy transformations. The energy spectrum of atmospheric turbulence can be divided into three sections: the energy-containing range, the inertial subrange and the dissipation range. In the first of these ranges energy is created, in the second one energy moves to the smaller eddies, while in the last one it is converted to thermal energy. This structure is sometimes referred as energy cascade of atmospheric turbulence.

2.4 Air-sea gas transfer

Wind-driven mixing produces an oceanic mixed layer, where water is well-mixed and the vertical profiles of variables are nearly constant(Stewart 1997, Chapter 6). Heat fluxes and turbulence shape the mixed layer: a change in temperature of mixed layer changes the water density and turbulence moves the heat downwards. The mixed layer is thinnest in late summer due to the low wind speeds and high solar radiation resulting in a layer of only a few meters thick whereas the mixed-layer thickness has its maximum in late winter. Solar radiation, mixing and stratification affect the CO_2 vertical profile in surface water.

Henry's law states that "a given concentration of the gas on the air side of the interface has to be in thermodynamic equilibrium with the concentration on the water side."(Csanady 2001, p. 44):

$$K_0 p = C_0, \tag{3}$$

where K_0 is the aqueous phase solubility, p is partial pressure of the given gas and C_0 is concentration at the surface of the water. Mass boundary layers exist in both sides of the surface (Fig. 5). The thicknesses of

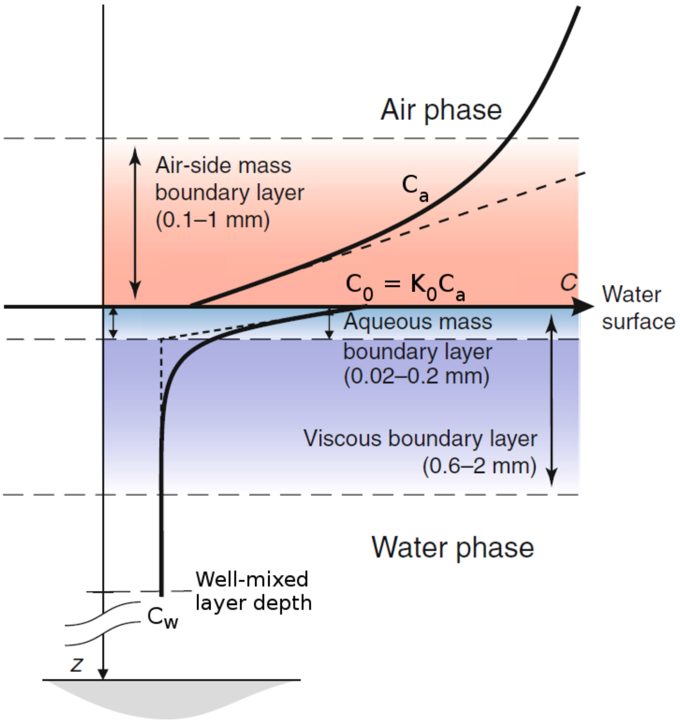

Figure 5: The gas exchange in the air-sea interface(Garbe et al. 2014). Modified symbols. Instead of using a partial pressure of carbon dioxide in the air, as in the text, the concentration of carbon dioxide in the air, C_a, is used.

these layers are altered by the interplay of molecular diffusion with eddies(Csanady 2001, p. 45). The transport across the interface happens through molecular diffusion. Turbulence causes the thicknesses of the layers to decrease thus increasing the exchange. The total resistance of gas exchange through the interface is the sum of the resistances in both mass boundary layers. For CO_2, the resistance of the aqueous side dominates due to low water-side diffusivity and low solubility(Garbe et al. 2014).

The gas exchange of a slightly soluble unreactive gas, e.g. carbon dioxide, between the atmosphere and the sea depends on the potential gradient, i.e. concentration difference, and the resistance, expressed here in terms of gas transfer velocity:

$$F_{\mathrm{CO}_2} = k(C_w - C_0), \tag{4}$$

where F_{CO_2} is the flux of carbon dioxide, k is the gas transfer velocity and C_w is the concentration in the bottom of the well-mixed layer. Eq. (4) can be expressed by using the partial pressure of CO_2 in the surface of the water that is in equilibrium with the air, pCO_{2a}, and the partial pressure of CO_2 in the bottom of the well-mixed water layer, pCO_{2w}:

$$F_{CO_2} = kK_0(pCO_{2w} - pCO_{2a}). \tag{5}$$

The simplest theory describing the gas exchange is the stagnant film theory. In this model the gas exchange is seen to be caused by the molecular diffusion in a thin layer. Then, the gas transfer velocity is the ratio of molecular diffusivity, D, to the thickness of the layer, δ: $k = \frac{D}{\delta}$. However, the research has shown that the gas exchange velocity actually depends on the fractional power of diffusivity(Wanninkhof et al. 2009). A more realistic description would take into account the change of the thickness of layer.

For relatively insoluble gas like CO_2, Garbe et al. (2014) list processes and properties, that affect the gas transfer: micro scale wave breaking, small and large scale turbulence in the water, waves, bubbles, sea spray, rain and surface films. At the low to moderate wind speeds, the turbulence generated by microscale wave breaking, i.e. breaking of of very short wind waves, is the dominant factor affecting the gas transfer. Besides altering the wave field, the wind also generates turbulence at the air-sea interface. For poorly soluble gases, the most important factor is the "bubble-mediated transfer", which describes the net transfer caused by the submerging bubbles. Also, surfacing bubbles create turbulence. Precipitation generates turbulence on the water surface, which increases the gas exchange. On low wind speeds, surfactant films can form a barrier to gas exchange. Also, surface-active material reduces the roughness of the sea and decreases the gas transfer by reducing micro-scale wave breaking and lowering the turbulence. For example, Phytoplankton can exude surface-active material. Biological processes, such as hydration of CO_2, influence the flux by changing the concentration gradient.

Apparently, many factors affect the magnitude of the gas transfer velocity, but in the case of open sea, wind speed is most commonly used for parametrization of k. Even though many theoretical approaches have been developed, the most common relationships between the flux and the wind speed are empirical. One of the most commonly used relationships between steady wind speed and gas transfer velocity is the formula presented by Wanninkhof (1992):

$$k = 0.31{U_{10}}^2(\frac{\mathrm{Sc}}{660})^{-1/2} \tag{6}$$

where U_{10} is the wind speed at a height of 10 m, Sc is the Schmidt number for CO_2, which describes the ratio of viscosity to diffusivity. The equation is normalized with Schmidt number in seawater at 20 °C, 660. Wind speed is expressed in m s^{-1} and gas transfer velocity is expressed in cm h^{-1}.

Garbe et al. (2014) note that since wave breaking depends on the wave steepness, it cannot be parametrised by wind speed alone. Wind speed, fetch, basin geometry, depth and atmospheric stratification have an effect on the wave field. The mean square wave slope has been suggested as a parametrization for gas transfer velocity.

2.5 Eddy covariance method

Any scalar or vector quantity, ζ, in the atmosphere follows the conservation equation:

$$S_\zeta = \frac{\partial \rho_d \zeta}{\partial t} + \nabla(u\rho_d\zeta) + D_\zeta \nabla^2(\rho_d\zeta) \tag{7}$$

where ρ_d is the density of dry air, u is the wind velocity, D_ζ is the molecular diffusivity of the quantity. The left side represents the sink/source strength. The equation states that the rate of change of the quantity can be caused by advection, molecular diffusion or production/absorbtion. A source produces, and a sink absorbs. When ζ is the velocity, one obtains

Navier-Stokes equation. Over flat and homogenous terrain, the molecular transport can be neglected(Foken et al. 2012a). For a scalar, e.g. the mixing ratio of a trace gas, χ, the equation simplifies:

$$S_\zeta = \frac{\partial \rho_d \chi}{\partial t} + \nabla(u \rho_d \chi) \tag{8}$$

A measured quantity can be separated into an average part and a fluctuation part: $\zeta = \bar{\zeta} + \zeta'$. This is called Reynold's decomposition. By applying Reynold's decomposition to the scalar conservation equation and taking an average of it, the equation takes the following form:

$$\overline{S_\chi} = \overline{\rho_d} \overline{\frac{\partial \chi}{\partial t}} + \overline{\rho_d u} \nabla \bar{\chi} + \nabla[\overline{\rho_d} \overline{u'\chi'}] \tag{9}$$

Now, the source term depends on the rate of change of the mixing ratio, advection due to gradients and divergence of eddy fluxes.

Next we assume the constant dry air density and integrate the equation over a volume. In addition, horizontal gradients are assumed to be neglible, and the measured quantities are assumed to represent the whole volume. The average net/sink strength in the volume (in the case of CO_2, so-called net ecosystem exchange, NEE) is now

$$NEE = \int_0^h \bar{\rho}_d \overline{\frac{\partial \chi}{\partial t}} dz + \int_0^h \overline{\rho_d w} \overline{\frac{\partial \chi}{\partial z}} dz + \bar{\rho}_d \overline{w'\chi'}|_h, \tag{10}$$

where w is vertical velocity. The first term on the right represents the storage, the second one is the vertical advection and the third term is the turbulent flux at the top of volume. The vertical advection is often neglible, and under steady-state conditions the storage term can also be neglected. This leads to the outcome that the sink/source strength can be estimated as vertical eddy covariance. It should, however, be noted that the equation works only when the turbulence is fully developed(Foken et al. 2012a).

In general, the covariance is calculated for a period long enough to take into account the largest eddies. The fluctuations required for the covariance are obtained by subtracting the mean value from the instantaneous values. Then, the mean of the product of fluctuations is calculated.

If one uses a closed-path gas analyzer - described in the next section - to measure carbon dioxide concentration, the lag caused by the tubing needs to be accounted for.

As shown above, the exchange of an atmospheric property between the atmosphere and the surface, the flux, can be measured with the eddy covariance method, if the high-frequency fluctuations of the atmospheric property can be measured in the atmospheric surface layer. If the assumptions outlined above can be satisfied, it is the most accurate method to measure the air-sea carbon dioxide flux because it does not rely on the approximations of gas properties or turbulent structure of the boundary layer(Wanninkhof et al. 2009). Unfortunately, it is also the most challenging method to measure sea-air exchange of CO_2 due to the low signal-noise-ratio. Rapid and accurate concentration and wind speed measurements are required to capture the smallest eddies. The theory behind the eddy covariance method has been known for a long time but it was not until the acoustic anemometers and high-frequency infrared gas analyzers had been developed that accurate and continuous measurents of carbon dioxide and water vapor fluxes were possible(Foken et al. 2012a).

2.5.1 Gas analyzer

When using the EC-method to measure the fluxes of CO_2, a fast-response gas analyzer is used to measure carbon dioxide and water vapour concentrations, in addition to a fast-response anemometer. Most of the carbon dioxide gas analyzers used for EC-method are infrared gas analyzers, IRGAs(Munger et al. 2012). IRGA consists of an infrared source, a frequency filter and a detector. Water vapour and carbon dioxide absorb infrared light, and the detector measures the drop in the radiation intensity, which is a function of carbon dioxide and water vapour concentrations. Munger et al. (2012) point out that “proportionality between light absorbance and density depends on the temperature, the pressure and the composition of the sample matrix, especially its water content.”

There are two kinds of IRGAs: closed-path and open-path analyzers. The closed-path gas analyzer has a closed chamber, through which the measurement gas flows, whereas the source and the detector of an open-path gas analyzer are in the ambient air. To measure the drop in the radiation intensity due to the carbon dioxide or water vapour present, a reference measurement is needed. Closed-path IRGAs typically have a second chamber for reference measurement. A gas with known carbon dioxide and water vapor concentrations flows through the reference chamber. The open-path analyzer gets the reference using another frequency that is not absorbed by CO_2 and H_2O.

There are pros and cons for both types of gas analyzers. Generally, closed-path analyzers are influenced by the high frequency turbulent energy loss caused by tubings, whereas the corresponding loss in open-path analyzers is smaller. Sensor separation between the open-path IRGA and the anemometer can cause high frequency turbulent energy loss. Munger et al. (2012) state that the distance between the anemometer and gas analyzer should be less than the size of the smallest eddies. In the case of closed-path instrument, the water vapour signal may be smoothed due to the contamination by hydrophilic material in the tubing. On the other hand, the closed-path analyzer works in severe weather, whereas open-path analyzer is inoperable when the lenses are wet, whether this is caused by precipitation, sea spray or condensation.

Munger et al. (2012) note that by minimizing the length of tubing and cleaning it regularly, one can minimize the problems of closed-path analyzer. However, to shorten the tubing requires that the analyzer is placed near the anemometer, which can be technically difficult and may distort the flow in some cases. Also, Blomquist et al. (2014) state that the long sample lines do not attenuate CO_2 fluxes if the flow rates are high.

Using the results from a decade of published work, Blomquist et al. (2014) conclude that "water vapour cross-sensitivity is the greatest source of error for CO_2 flux measurements using infrared gas analyzers". Cross-sensitivity effect consists of pressure broadening effect and direct absorption interference caused by spectral overlapping of CO_2 and H_2O. The use of a sample air dryer and a closed-path gas analyzer is suggested to eliminate this effect most effectively.

2.5.2 Flux tower and footprint

The anemometer and the inlet of the gas analyzer, or the whole gas analyzer in the case of open-path, are attached into a mast, i.e. a flux tower. Munger et al. (2012) note that the area of interest, prevailing winds and flow distortion among other things should be considered when positioning the tower. The height of the tower should be high enough so that the measurements are taken in a well-mixed surface layer where they are not influenced by the roughness layer or individual canopies. Also, the tower cannot be that high it is beyond the surface layer during stable night-time conditions(Munger et al. 2012).

The area that the flux measurement represents is called the flux footprint. The measured CO_2 flux is a combination of the effects of all sinks and sources of carbon dioxide within the footprint area. It is mostly located on the windward side of the flux tower and depends on the measurement height, the atmospheric stability and the wind speed. Rannik et al. (2012) demonstrate that the more unstable the surface layer gets, the closer the footprint is located. This is due to the increased turbulence. During the neutral and stable conditions, the footprint is located further away from the flux tower and is distributed more evenly. Figure 6 illustrates the basic idea of footprint by showing the crosswind-integrated footprint distribution. The distribution is asymmetric and the area closest to the tower has a minimal contribution to the flux.

To describe the flux between the atmosphere and the sea, ideally the flux tower should be placed on a platform in the sea. A ship or a buoy are possible options. The motion of the platform is a problem for accurate flux measurements, and the motion effect has to be corrected. In the case of ships, complex distortions are formed in the flow field, which can be prevented by special ship design. Norman et al. (2011) report

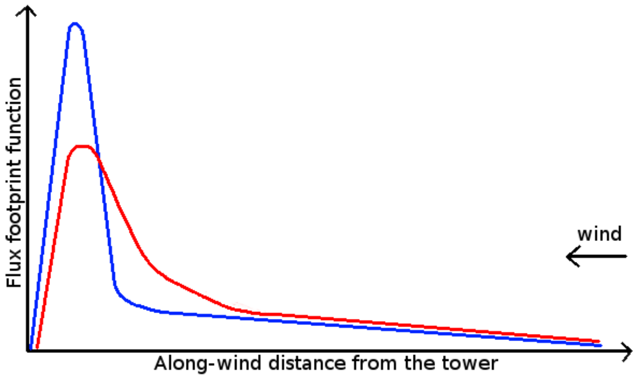

Figure 6: Schematics of croswind-integrated flux in unstable conditions (blue line) and stable conditions (red line).

that the movement of the ship or platform can produce a spike in the spectrum at the frequency band 0.1–1 Hz. Additionally, it can be difficult to build tower tall enough at the platforms and they rarely are capable of long-term measurements(Högström et al. 2008). Högström et al. (2008) showed that a flux tower placed on the shore can be used measure the sea-air interaction when the wind is blowing from the sea.

2.5.3 Data processing

Eddy covariance is an accurate method to measure carbon dioxide fluxes but only if used properly, as it requires extensive data processing and multiple corrections to be applied. Some of the corrections are usually done automatically while others may need manual labour.

The coordinate system is typically rotated so that the mean vertical velocity is forced to zero. This also serves as a correction for a potential tilt of the anemometer. The data needs to be de-spiked for technical errors. The anemometer detects the so-called acoustic temperature, which is corrected for the wind effects, after which it is transformed to actual air temperature. The signals from different instruments must be synchronised. This involves finding the delay time, or the lag, between the anemometer and the closed-path analyzer data streams.

The high frequencies are attenuated, e.g. due to the imperfect sensor response, sensor separation and the air transport through the tubes(Foken et al. 2012b). On the other hand, the averaging period, usually 30 minutes, may be too short to include the lowest frequencies involved in turbulent transfer. The corrections for such spectral limitations can be done theoretically or experimentally. The experimental approach rests on the assumption that the covariance of vertical velocity, w, and air temperature, T_a, is unattenuated. Thus, co-spectrum of vertical velocity and air temperature, Co_{wT}, can be used as a reference to correct the carbon dioxide flux.

Fluctuations in temperature and humidity influence the fluctuations of trace gas concentrations. The so-called WPL-correction - after the three authors Webb, Pearman and Leuning - is used to remove this effect. Foken et al. (2012b) report that the correction reduces significantly the carbon dioxide flux calculated directly from the covariance. The need for the correction arises from the fact that instruments usually measure densities instead of mixing ratios. WPL-correction is derived from the conservation equation, Eq. (10). Open-path system needs to be corrected for the effect of both temperature and water vapor fluxes. In the case of closed-path systems, thermally conductive tubings eliminate the temperature fluctuations, and only water vapor flux correction is needed. It is preferred that closed-path instrument can compute the dry air mole fraction in real time, thus eliminating the need for density corrections.

There also exists other corrections that may be necessary for specific instruments. The open-path gas analyzer LI-7500 (Li-cor) has a heater on its sensor head, and the heating can produce convection, which may need to be taken into account(Foken et al. 2012b).

During the night time the BL often gets a stable structure and carbon dioxide fluxes can be underestimated in such conditions due to weak mixing(Foken et al. 2012b). When the turbulent mixing is suppressed, the importance of storage and advection terms in Eq. (10) increase and cannot be disregarded anymore. These observations are usually discarded, by using too low friction velocity as a criterion(Aubinet et al. 2012).

3 Materials and methods

3.1 Site description

3.1.1 Location

The Archipelago Sea is located between the Sea of Åland and Finland. It is shallow, typically under 40 m deep, and it comprises of thousands of small islands(Myrberg et al. 2006, p. 54).

Utö is an island located at the sourthern edge of the Archipelago Sea, at $59° 46,5'$N, $21° 22,2'$E (Fig. 7). Utö is the southernmost inhabited island of Finland. The island is equipped with electricity, running water and internet. A ferryboat travels between Utö and mainland multiple times a week. All of this makes it possible to carry out measuring campaigns and maintenance of long-term monitoring measurements effortlessly. Also, Utö has a long history of meteorological and oceanographic measurements. The Finnish Meteorological Institute has carried out meteorological measurements on Utö since 1881, and since 1900, seawater temperature and salinity measurements have been carried out(Finnish Meteorological Institute 2015).

The construction of the new Atmospheric and marine research station was started in 2012. It is being built by the Finnish Meteorological Institute with collaboration of the Finnish Environment Institute. It locates within a military area on the western side of the island. A micrometeorological tower is next to the station, and the inlet for the flow-through pumping system is located 250 m west from the station. As a part of the Integrated Carbon Observation System(ICOS), the new station will observe the carbon dioxide concentration in the surface layer of the sea and CO_2 fluxes between the sea and the atmosphere(Finnish Meteorological Institute 2017). The precise atmospheric CO_2 concentration measurements, together with CO and CH_4 measurements, are carried out for the ICOS network in the south-eastern part of the island.

To measure trace gas concentrations and fluxes the station has a micrometeorological tower equipped with eddy covariance instrumenta-

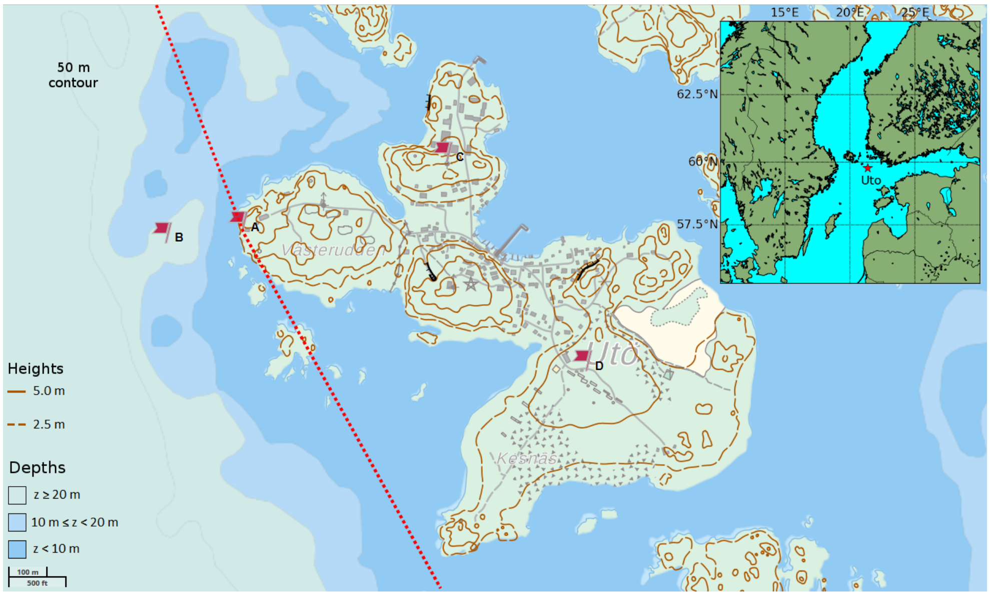

Figure 7: The location and topography of Utö. New atmospheric and marine research station (A), inlet of flow-through pumping system (B), ICOS atmospheric carbon dioxide concentration measurement site (C) and meteorological station (D). The red dashed lines represent the open sea sector that is determined in the results.

tion(Fig. 8). At the feet of the tower, there is a small hut to keep instruments and a computer dry and warm. The sea is located to the west of the station, and about a 0.5 km west from the station the sea floor quickly deepens to about 80 m. The height of the tower is 8 m and the small hut is 1.5 m tall. The water level is approximately 5 m lower than the base of the tower and the hut. The area has no trees, but the cliff gets higher when moving further away from the shore. The tower and the small hut are portrayed in fig. 8. The figure shows the frequently occurring hard weather and sea spray that the setup needs to cope with.

Figure 8: The flux tower in the middle of the figure and the instrument hut at the feet of it (Ismo Willström).

3.1.2 Climatology

Typical for a small island, the surrounding sea has a stabilizing effect on the temperatures measured at Utö (Fig. 9). During the winter, the air temperature is close to zero. February is the coldest month with an average temperature of $-2.2\,°\mathrm{C}$, and the maximum temperature, $16.7\,°\mathrm{C}$, is reached in July(Pirinen et al. 2012). The seawater temperature follows closely the air temperature, but due to the high heat capacity of the water, the difference between maximum and minimum temperatures is slightly smaller for the sea.

The mean wind speed at Utö is $7.1\,\mathrm{ms}^{-1}$. In the summer, the wind speed has its minimum, $5.6\,\mathrm{ms}^{-1}$ in May and in July, whereas the average mean wind speed in December is $8.9\,\mathrm{ms}^{-1}$. The wind blows 20% of the time from the southwest and the highest annual mean wind speeds occur in the southwestern flow, $7.8\,\mathrm{ms}^{-1}$(Pirinen et al. 2012).

The mean annual precipitation at Utö is 549 mm. The highest precipitation values are recorded in the autumn, 65 mm in October, whereas

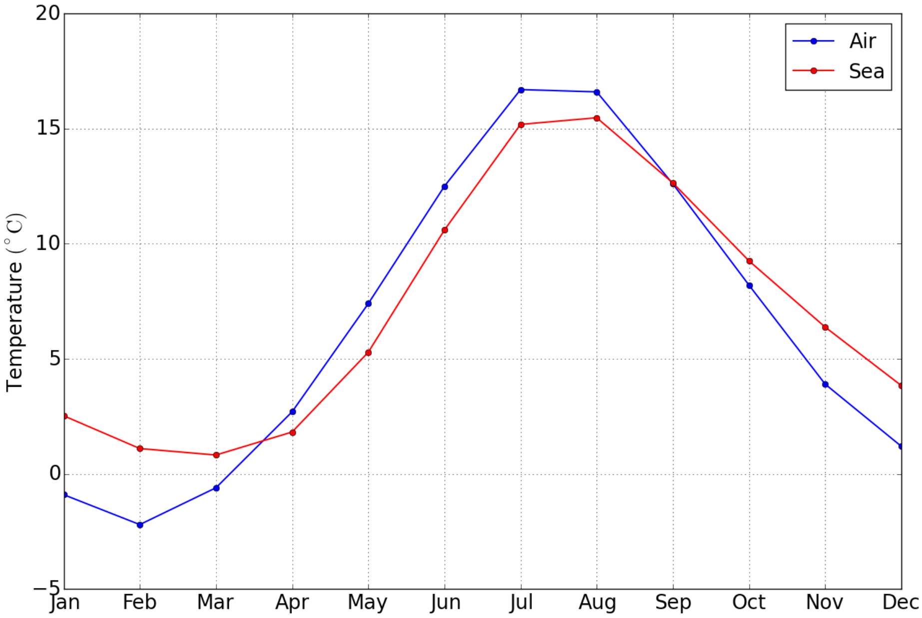

Figure 9: Air temperature at the height of 2 m(Pirinen et al. 2012) and seawater temperature at the depth of 5 m(Laakso 2017). The data of sea temperature is collected between 1971–2000, whereas the data of air temperature is from the years 1981–2010.

in April the mean precipitation is 26 mm(Pirinen et al. 2012).

There is sea ice around Utö for 0–4 months a year(Myrberg et al. 2006, p.139).

3.2 Measurements

3.2.1 Flux tower

A LI-7000 closed-path infrared gas analyzer (Li-cor) is used to measure carbon dioxide and water vapour concentrations. The instrument is placed in the hut and the gas inlet is located at the top of the tower, at the height of about 8 m (Fig. 10 and Fig. 11). This LI-7000 instrument is called in this study as IKO. Two other gas analyzers were used for comparison for flux measurements. These are another closed-path LI-

7000, called here MER, and a LI-7500 open-path infrared gas analyzer (Li-cor). A two months period of flux measurements, 14 October – 14 December 2016, was examined in this study. LI-7500 stopped working on 28th of October due to a possible chopper failure.

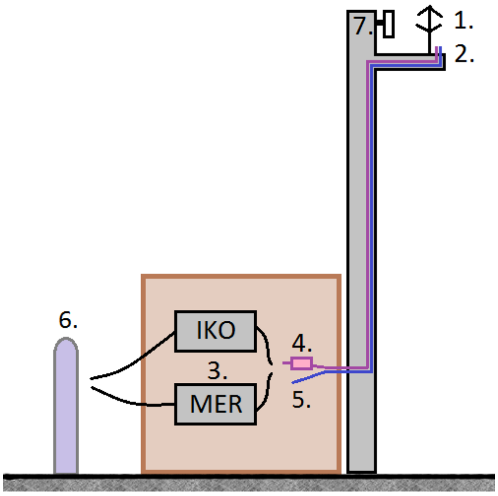

Figure 10: Closed-path gas analyzer setup: acoustic anemometer (1), gas inlet (2), gas analyzers (3), virtual impactor connected to a steel steel pipe line (4), teflon pipe line (5), reference gas container which is found in the station (6) and open-path gas analyzer (7).

The tubing of IKO is made of 4 mm diameter steel pipe and its length is approximately 10 m. MER has 3.175 mm Teflon tubing. Both pipe lines have Teflon filters to avoid water and particle contamination of the instruments. The steel pipe line is also equipped with a virtual impactor, which should protect the instrument from water if the teflon filter would fail. As saline water is a danger for a LI-7000(LI-COR 2005), the virtual impactor separates small particles from large particles with a perpendicular air flow. On the 28th of October, the pipe lines were swapped, and thus in the latter part of the study period the MER was connected to the steel pipe line and the virtual impactor. Both gas analyzers use an external pump providing a flow rate of 5.5–6.5 $\mathrm{l\,min^{-1}}$. Because the steel pipe had been in use for two years, we flushed the pipe with pure water and isopropyl alcohol in the beginning of the test period.

The Teflon pipe was brand new. Also, we cleaned the optical lenses of the analyzers, and the internal chemicals were also replaced.

We calibrated the gas analyzers with gases of known concentrations. A gas with zero carbon dioxide and water vapour concentrations (zero gas) and a gas with 364.4 ppm CO_2 concentration (span gas) were used to calibrate the gas analyzers. The water vapour concentration of the span gas was unknown, and the span vapour calibration was not set, which could have had an effect on the accuracy of water vapour concentration measurements.

Figure 11: The top of the flux tower. From top to bottom: LI-7500 (Li-cor) open-path gas analyzer (1), uSonic-3 (Metek) anemometer (2) and the inlet for closed-path analyzers (3).

Wind velocity was measured with uSonic-3 (Metek) acoustic anemometer. The carbon dioxide fluxes are calculated on-line with the PyBarFlux software of the Finnish Meteorological Institute. All the above mentioned corrections are applied, excluding the spectral flux loss correction. Low turbulent data was discarded when the friction velocity could not have been calculated. Obvious outliers were discarded.

By inspecting the surface roughness calculated from the data as a function of wind direction, we determined the wind directions that represent the open sea area. The surface roughness was calculated using Eq. (1) for neutral conditions, here defined as $|1/L| < 0.01\mathrm{m}^{-1}$.

To examine the high-frequency response of the instruments, I wrote a Python script that calculates the cospectrum of CO_2 and w, Co_{wC}. Also, the cospectrum of T_a and w, Co_{wT}, was calculated and it was taken as a reference for evaluating Co_{wc}. In the spectral analysis, CO_2 mixing ratios with respect to dry air were used, w and v were forced to be zero, spikes larger than six times the standard deviation were removed. Linear detrending was used, and Hanning window was applied. Discrete fast fourier transform by Python-based software Scipy was performed. The cospectra were normalized with covariances. The spectra were divided so that in the logarithmic scale the points would be equally spaced. The frequency was normalized with the measurement height and the wind speed:

$$n = f\frac{U}{z}, \tag{11}$$

where n is the normalized frequency and f is frequency in Hz. To quantify the high frequency loss, a half power frequency, f_0, was determined by fitting a transfer function to the ratio of C_{wc} to C_{wT}. A gaussian transfer function was selected for this purpose:

$$T_{wC} = \exp[-\ln(2)(\frac{f}{f_0})^2] \tag{12}$$

After the measuring period, we noticed that the CO_2 concentrations measured with LI-7000 instruments were linked to the variations in the internal instrument temperatures. To quantify the relationship between the instrument temperature and CO_2 concentration offset, we measured the concentration of the calibration gas for 90 min while slowly cooling down the instruments on 16 January 2017. The CO_2 molar fraction of the calibration gas was 364.4 ppm. The cooling of the instrument was induced by turning down the heater of the hut.

3.2.2 Flow-through pumping system

The station is equipped with a state-of-the-art flow-through pumping system of seawater. The pump is located about 250 m from the shore (Fig. 12). The pump is at a depth of 23 m. The inlet is kept at a depth of 5 m with buoys, therefore the measurement does not technically represent the surface water conditions. The flow rate is about 30 $\mathrm{l\,min^{-1}}$, and the residence time of water is about 24 min.

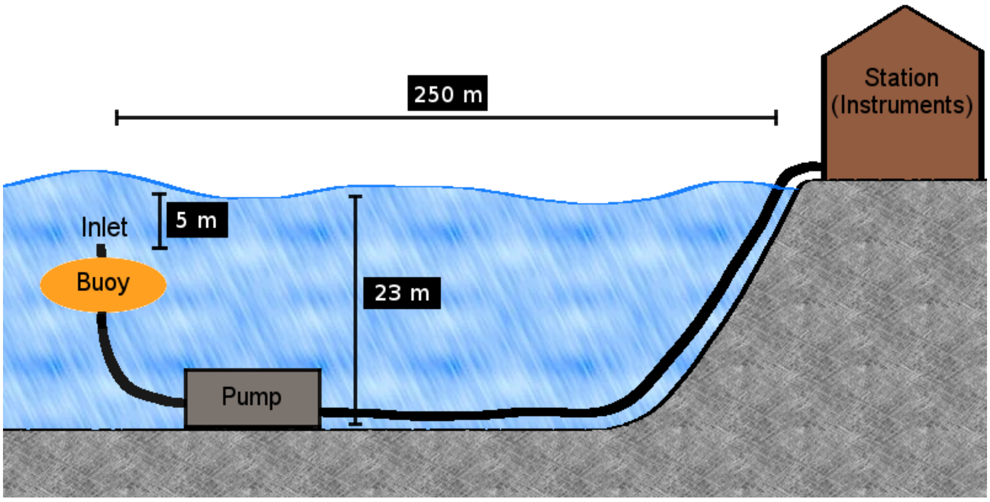

Figure 12: Schematic picture of the pumping system.

The dissolved carbon dioxide concentration is measured with a combination of two equilibration chambers and an IRGA, $\mathrm{SuperCO_2}$ (Sunburst Sensors), connected to the flow-through pumping system. In the equilibration chambers carbon dioxide is equilibrated between the sample water and air by using the showerhead technique. After this the gas is directed to a LI-840A closed-path gas analyzer (Li-cor). For every four hours, four different calibration gases are directed through the system.

I wrote a Python script to correct the measured molar fraction values by using the calibration measurements. For every calibration sequence, the script calculates a linear regression function between the measured molar fractions and the real molar fractions. The equilibration chamber is regularly and automatically cleaned with hydrogen peroxide.

Seawater salinity and temperature are measured with a MicroTSG SBE 45 thermosalinograph (Sea-bird Scientific). The pH of sea water is measured with an AFT-pH instrument (Sunburst), which uses the colorimetric reagent method. The pH instrument was only operating during 5 July – 3 October 2016.

Since pH and dissolved carbon dioxide were measured simultaneously, we were able examine the whole aquatic inorganic carbonate system:

$$\begin{aligned}
[\mathrm{H^+}] &= 10^{-\mathrm{pH}} \\
[\mathrm{OH^-}] &= \frac{K_w}{[\mathrm{H^+}]} \\
[\mathrm{HCO_3}^-] &= \frac{K_1[\mathrm{CO_2}]}{[\mathrm{H^+}]} \\
[\mathrm{CO_3}^{2-}] &= \frac{K_2[\mathrm{HCO_3}^-]}{[\mathrm{H^+}]} \\
\mathrm{TA} &= [\mathrm{HCO_3}^-] + 2[\mathrm{CO_3}^{2-}] + [\mathrm{OH^-}] - [\mathrm{H^+}] \\
\mathrm{TIC} &= [\mathrm{HCO_3}^-] + [\mathrm{CO_3}^{2-}] + [\mathrm{CO_2}],
\end{aligned}$$

where K_w is the equilibrium constant of water, K_1 is the first dissociation constant of carbonic acid and K_2 is the second dissociation constant. The constants are calculated according to Millero (1995). Square brackets denote concentration. The concentration of the dissolved CO_2 is calculated using the Henry's law, Eq. (3).

During 20 – 28 August, the filter of the equilibration chamber of SuperCO_2 was clogged and the data during that time is discarded. During 16 – 26 November, the computer in charge of saving the thermosalinograph data had a malfunction and there is no salinity or seawater temperature data from that period. In addition to these, there are some periods of unavailable data due to maintenance. Also, periods of calibration and automatic cleanups were removed from the time series.

3.2.3 Supporting data

For atmospheric CO_2 concentration measurements we use the data obtained from a G2401 high-precision analyzer (Picarro) as a reference. The instrument uses very stable cavity ring-down spectroscopy. The concentration measurement site is located on the north side of the island, approximately 600 m away from the atmospheric and marine research station. The inlet for the analyzer is at a height of 56 m, therefore it does not technically represent the surface conditions over the sea.

An automatic weather station on the island provides supporting meteorological data. It is located approximately 1 km away from the new atmospheric and marine research station. The weather station is equipped with a 10 m tall wind tower. The terrain around this station is even and there are no high obstacles around it.

3.2.4 Air-sea CO_2 flux calculation using the parametrization

The measured carbon dioxide fluxes were compared with the fluxes calculated using wind speed-flux-relationship based on Eq. (5) and Eq. (6). For this, the atmospheric CO_2 concentration is obtained from Picarro G2401 and the dissolved carbon dioxide concentration is from SuperCO_2. For calculating partial pressures of CO_2 from molar fractions, atmospheric pressure measured at the weather station is used. The CO_2 solubility is calculated from seawater temperature and salinity, both measured with the flow-through pumping system, according to Weiss (1974). The seawater temperature is also used to calculate the Schmidt number of CO_2 according to Wanninkhof (1992).

Eq. (6) uses the wind speed at a height of 10 m, so the wind speed was corrected based on the logarithmic wind profile:

$$u_{10} = u_8 \frac{\log(\frac{10\,\mathrm{m}}{z_0})}{\log(\frac{8\,\mathrm{m}}{z_0})} \tag{13}$$

The average roughness length of neutral conditions, $|1/L| < 0.01\mathrm{m}^{-1}$, is used. No stability correction was used since the BL was nearly neutral most of the time.

4 Results and discussion

4.1 Environmental conditions

As the measuring period was during the late autumn, temperatures of air and sea water decreased during the measuring period (Fig. 13). The sea temperature decreased rather linearly from 10.8 °C to 4.3 °C, whereas the air temperature had naturally more variation. The air temperature decreased from approximately 4 °C to 0 °C. Temperature of the maximum density for seawater, about 3 °C for seawater with salinity of 6 g kg^{-1}, was not reached and the deepening of the mixed layer had not yet occurred. However, it should be noted that the temperature readings from flow-through pumping system may be biased since the sample water may cool or warm during the flow inside the tube.

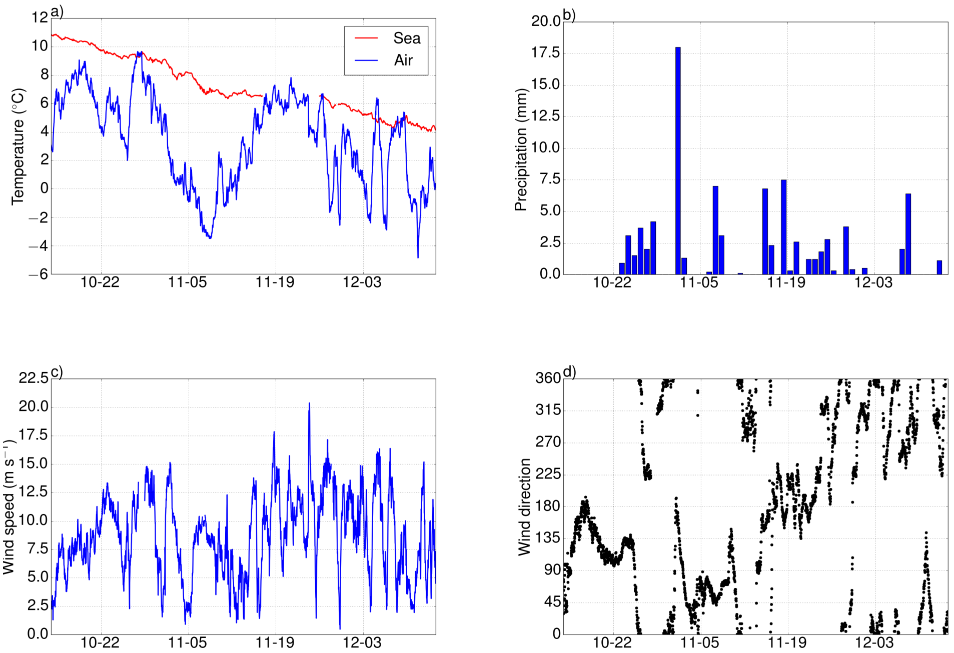

Figure 13: a) Sea temperature at a depth of 5 m and air temperature at a heigth of 2 m, b) daily precipitation, c) wind speed and d) wind direction during 14 October - 14 December 2016.

During the measurement period, precipitation was frequent, excluding the first week that had no rain. It rained 60.7 mm in November, which is close to the average monthly average precipitation of November, 63 mm(Pirinen et al. 2012).

The mean of wind speed was 9.0 ms^{-1} with a standard deviation of 3.4 ms^{-1}. In the beginning of the period wind was blowing from the southeast for about 7 days. After that the wind direction turned to the northeast. At the end of November the wind blew from the south. During the last couple of weeks the wind was blowing from the north and northwest.

The anemometer directions had not been calibrated previously. When compared to the meteorological station data, it was found out that directions showed 21.5° too much clockwise and this error was corrected in the results.

The stability was near neutral during the study: 90% of the time, stability parameter was between -0.03 and 0.003. Only a couple of times the stability was even slightly stable and the strongest stable stability recorded was 0.16.

To verify the validity of the wind measurements it is useful check if the universal relationships derived for the boundary layer flow apply. For instance, according to the Monin-Obukhov similarity theory there exists an unique relationship between the normalized standard deviation of vertical velocity, σ_w, and the stability parameter(Arya 2001, p. 237). The normalization is done by dividing the standard deviation with the friction velocity. The relationship proposed by Arya (2001, p. 237) is:

$$\frac{\sigma_w}{u_*} = 1.25[1 - 3(z/L)]^{\frac{1}{3}} \tag{14}$$

This relationship is derived from multiple aircraft and tower data taken over land and sea surfaces. The best fit to the Utö data is similar to that of Eq. (14):

$$\frac{\sigma_w}{u_*} = 1.16[1 - 2.86(z/L)]^{\frac{1}{3}} \tag{15}$$

The coefficient of determination of this fit is 0.66. Both equations fit well to the present observations(Fig. 14). The observed $\frac{\sigma_w}{u_*}$ is clearly a func-

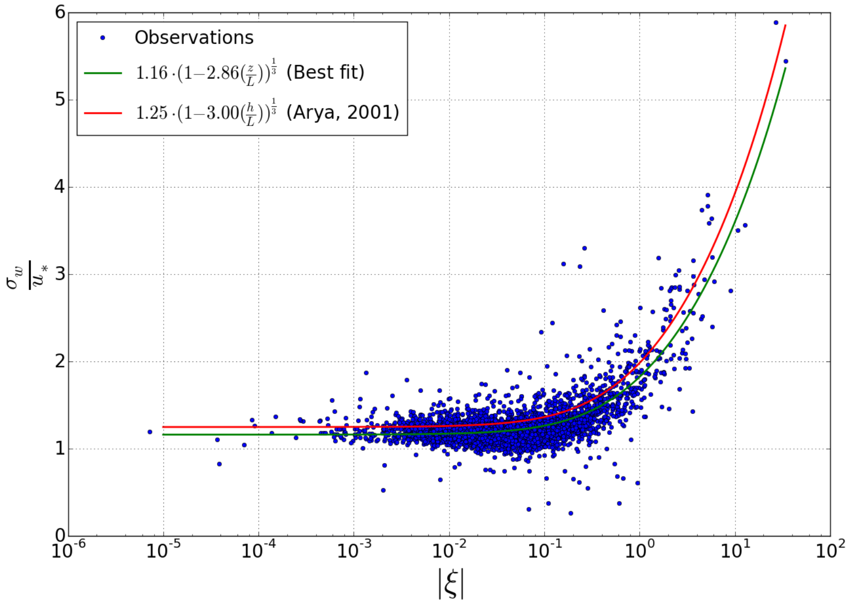

Figure 14: Normalized standard deviation of vertical velocity as a function of stability.

tion of the stability, and this so-called flux-variance similarity indicates development of atmospheric turbulent conditions(Foken et al. 2012b).

4.2 Atmospheric carbon dioxide

Generally, the atmospheric CO_2 partial pressure remained constant or slightly increased during the study (Fig. 15), which is in agreement with the annual cycle showing a low photosynthetic activity at the end of the year. At the beginning of the period the partial pressure of CO_2 measured by Picarro was 412 µatm, and at the end of the period it was 413 µatm. The sudden changes in atmospheric concentrations are most likely related to the wind direction changes, since the changes in air-sea flux of CO_2 do not coincide with the changes in atmospheric CO_2 concentration. On the 27th of October wind started to blow from the southwest and the partial pressure increased by 11 µatm and by dropped 22 µatm when direction turned to the north. A 19 µatm drop was observed when the wind started to blow steadily from the south on 16 November. There is a large peak on the 8th of December: the partial pressure increased 15 µatm rapidly when wind was blowing steadily from west. Increase in concentration under western winds could be caused by anthopogenic emissions in Sweden.

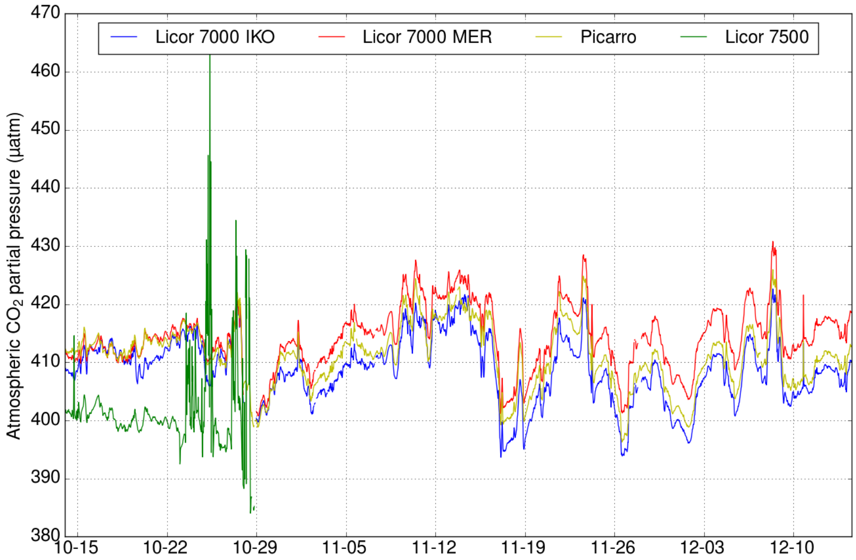

Figure 15: Atmospheric carbon dioxide partial pressure during 14 October - 14 December 2016.

While concentration measured by Picarro remained almost constant during 19–23 October, the concentration measured by LI-7500 decreased by 5 µatm. Also, the concentration offset between LI-7500 and other instruments is quite alarming, 10 µatm at the beginning of the period. After 23 of October precipitation was frequent and the concentration values of LI-7500 readings are very noisy. Apparently, the instrument is very sensitive to precipitation. According to LI-COR (2002), rain and snow affect the performance of the instrument. False readings can be caused by total blockage of the sensor by droplets or flakes, or the reference measurement may be blocked but the sample measurement is not, or vice versa.

Closed-path instruments follow the reference instrument Picarro bet-

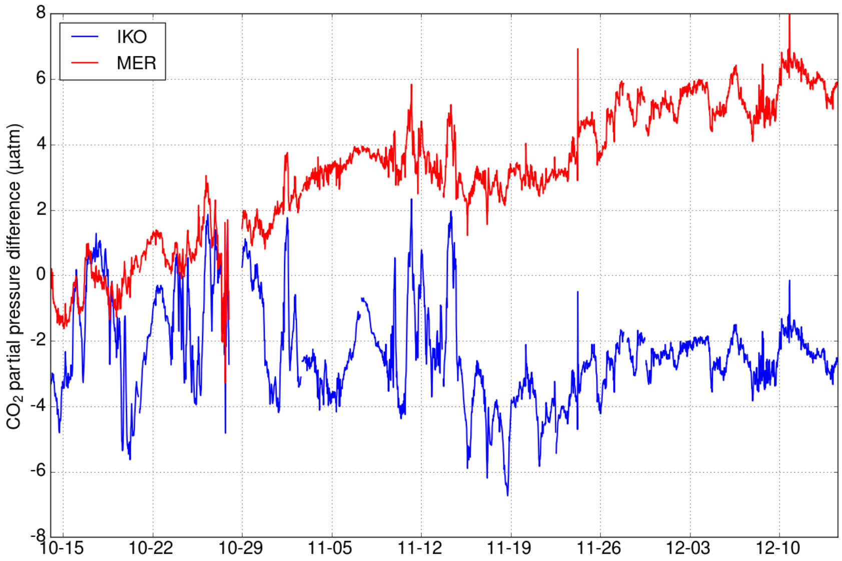

Figure 16: The time drift of LI-7000 instruments determined as a difference from Picarro during 14 October - 14 December 2016.

ter. The concentration of the IKO follows very well the Picarro reference analyzer. It is always slightly smaller, typically 2 µatm, than the reference and the difference between the instruments seems to vary randomly (Fig. 16). The MER instrument, on the other hand, shows some temporal drift: right after the calibration the concentration difference between MER and Picarro was small but it increased with the time to 6 µatm. This indicates that the temporal drift depends on the instrument. More frequent calibrations are needed if exact concentration measurements are needed.

Because the wind speeds were rather high and the structure of the boundary layer was not stable, even during the nighttime, we assumed that the data from Picarro and Licors are comparable. In very stable conditions, Picarro positioned at a height of 56 m could measure concentrations above the boundary layer.

We found out that both LI-7000 instruments are sensitive to instru-

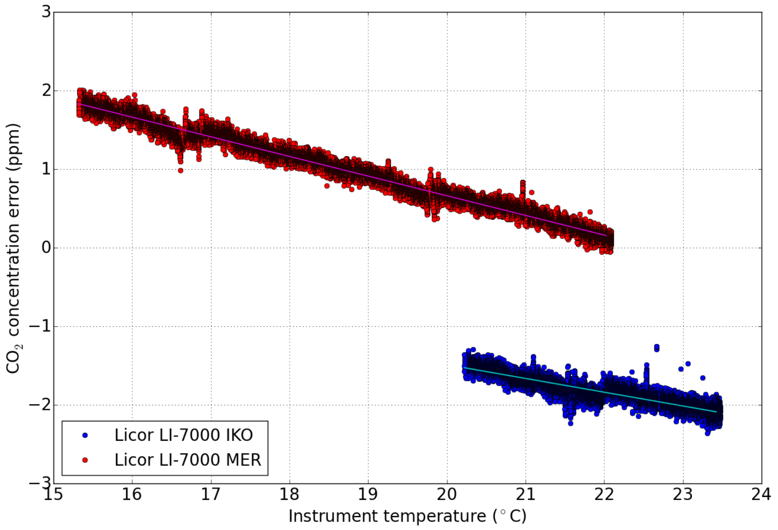

Figure 17: The molar fraction error as a function of instrument temperature.

ment temperature changes (Fig. 17). This affects more MER instrument:

$$\epsilon_{IKO} = -0.18\,\mathrm{ppm}^{\circ}\mathrm{C}^{-1} \cdot T_i + 2.02\,\mathrm{ppm} \tag{16}$$

$$\epsilon_{MER} = -0.25\,\mathrm{ppm}^{\circ}\mathrm{C}^{-1} \cdot T_i + 5.67\,\mathrm{ppm} \tag{17}$$

where ϵ is the molar fraction error and T_i is instrument temperature. The error was calculated by subtracting the known calibration gas molar fraction from the measured molar fraction. LI-COR (2005) states that LI-7000 can take the temperature effect into account and the typical error is $0.3\,\mathrm{ppm}\,^{\circ}\mathrm{C}^{-1}$. MER almost has this strong temperature drift, $0.25\,\mathrm{ppm}\,^{\circ}\mathrm{C}^{-1}$. The temperature dependence in IKO, on the other hand, may have been compensated better, with only a $0.18\,\mathrm{ppm}\,^{\circ}\mathrm{C}^{-1}$ slope. This temperature dependence would explain the apparently random difference with Picarro during the measuring period(Fig. 16).

4.3 Dissolved carbon dioxide

The changes in CO$_2$ partial pressure in the sea are much greater than the changes in the atmospheric CO$_2$ partial pressure(Fig. 18). The minimum concentration, 110 µatm, measured in the late July represents the second annual growth of phytoplankton. After that the stratification breaks down quickly and CO_2-rich water surfaces in the beginning of August. However, stratification develops quickly during calm September causing CO_2 partial pressure in surface water to decrease. High winds in autumn raise the concentration level back to 500–600 µatm, where the level stays for the rest of the year.

Figure 18: The dissolved carbon dioxide during 5 July – 14 December 2016. The period marked with red vertical lines represents the time when pH was measured and the green vertical lines represent the flux measurement period.

As the partial pressure of dissolved CO_2 increased from 200 µatm to 600 µatm during the period, pH decreased from 8.5 to 7.9 at the same time. pH is clearly linked to dissolved CO_2 concentration (Fig. 19). An increment of dissolved carbon dioxide concentration causes acidification of sea water.

From the measured pH and dissolved carbon dioxide, we calculated the other components of the aquatic carbonate system. The mean total

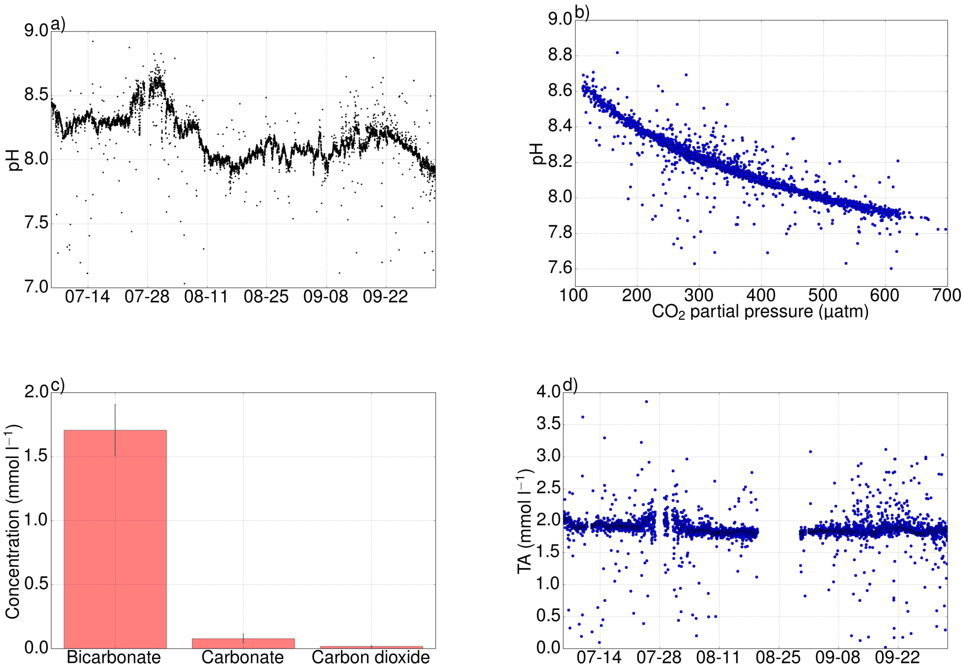

Figure 19: Different components of the inorganic carbonate system during July – October 2016: a) pH, b) pH as function of dissolved CO_2 partial pressure, c) Total inorganic carbon: mean constituents and standard deviations and d) Total alkalinity.

alkalinity was 1.87 $\mathrm{mmol l^{-1}}$ and it did not show large temporal variation. The total inorganic carbon concentration was only slightly lower than TA: 1.80 $\mathrm{mmol l^{-1}}$. Thomas and Schneider (1999) have concluded that Scandinavian waters are characterized by low TIC and TA values due to low lime content in soils in the drainage area; e.g. for Northern Gotland Sea they measured TIC of approximately 1.46 $\mathrm{mmol l^{-1}}$ in mid November. The bicarbonate ion had the highest concentration in TIC, with an average of 1.70 $\mathrm{mmol l^{-1}}$ and a standard deviation of 0.2 $\mathrm{mmol l^{-1}}$. The mean carbonate ion and CO_2 concentrations were 0.04 $\mathrm{mmol l^{-1}}$ and 0.008 $\mathrm{mmol l^{-1}}$, respectively.

Since not all ions are taken into account when calculating the TA(e.g. hydrogen sulphate and borate), the calculated TA is only directional.

The influence of these ions could be studied by using titrimetric determination of TA.

4.4 Carbon dioxide flux

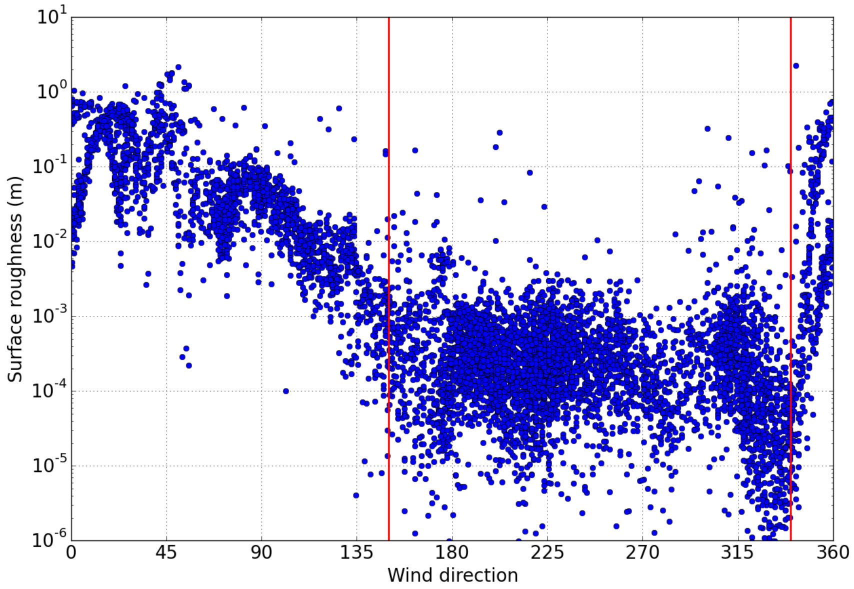

Figure 20: The surface roughness as a function of wind direction. The red lines represent the limits of the open sea sector.

The sector that is representative of the flow from the sea area was resolved by examining the surface roughness as a function of wind direction. Figure 20 shows clearly that the sector of 150–340° represents the sea area and these wind directions will be used when studying the air-sea gas exchange. The sea sector had a mean surface roughness of 1 mm, which indicates off-sea wind in coastal areas(Arya 2001, p. 199), whereas the mean surface roughness outside the above mentioned sector was 12 cm. These limits are in agreement with the sector deduced directly from the map. However, the northermost limit would not have been that easy to resolve from the map alone. In the southeast the 150° limit represents the southermost part of Utö (Fig. 7). The north limit of 340°, on the other hand, represents the new station. Also, the tower possibly has an effect on the flow for the northernmost winds as the anemometer is facing south. During the two months measuring period, 49 % of the time the wind was blowing from the sea sector.

4.4.1 Flux comparison

The air-sea fluxes of CO_2 during October-December 2016 were positive, meaning that the sea acted as a source of carbon dioxide (Fig. 21). This was expected since the partial pressure of CO_2 was larger in water than in air. Since the CO_2 partial pressure in the sea rose early in the autumn (Fig. 18) and exceeded atmospheric partial pressure, the sea became source early. The mean carbon dioxide flux from IKO during 14 October - 14 December 2016 was 0.313 $\mu mol m^{-2} s^{-1}$, whereas MER showed 0.250 $\mu mol m^{-2} s^{-1}$, so IKO had 25% higher mean than the MER. Heavily biased LI-7500 had a negative mean, -0.0102 $\mu mol m^{-2} s^{-1}$. The

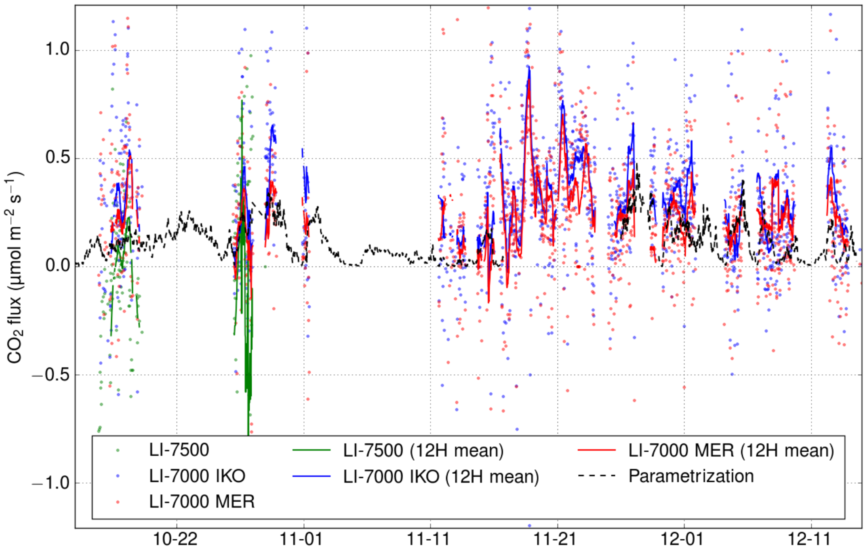

Figure 21: The measured carbon dioxide flux and the flux calculated using the parametrization of gas transfer velocity during 14 October - 14 December 2016.

standard deviations of the fluxes were similar: 0.452 µmolm^{-2}s^{-1} for IKO and 0.438 µmolm^{-2}s^{-1} for MER.

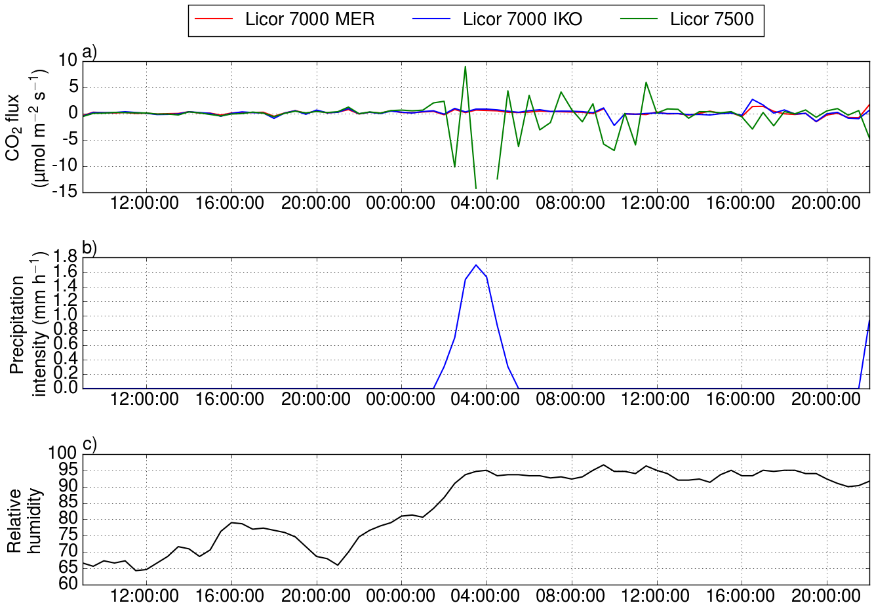

Figure 22: a) The CO_2 fluxes measured with different IRGAs, b) Precipitation intensity and c) Relative humidity during 26 – 27 October 2016.

The precipitation affects the readings of LI-7500 as opposed to the closed-path LI-7000 instruments; an example of this effect is shown in Fig. 22. The evening of 26th of October was clear and dry with a relative humidity under 80 %, but after midnight a shower occurred and instantly the CO_2 flux measured with LI-7500 started to oscillate heavily. Even after the rain, the reading did not stabilize, even though the instrument had been installed in a slightly tilted position, which would help the water to fall off. However, the relative humidity stayed high, 90–95 %, after the rainfall, which may have caused condensation on the surface of the optical path. No sea spray was observed during the period, but it would most likely cause similar problems with the open-path instrument. Precipitation and high relative humidity are easy to detect from weather data, but that would not be the case with the sea spray.

The two closed-path infrared gas analyzer set-ups showed similar

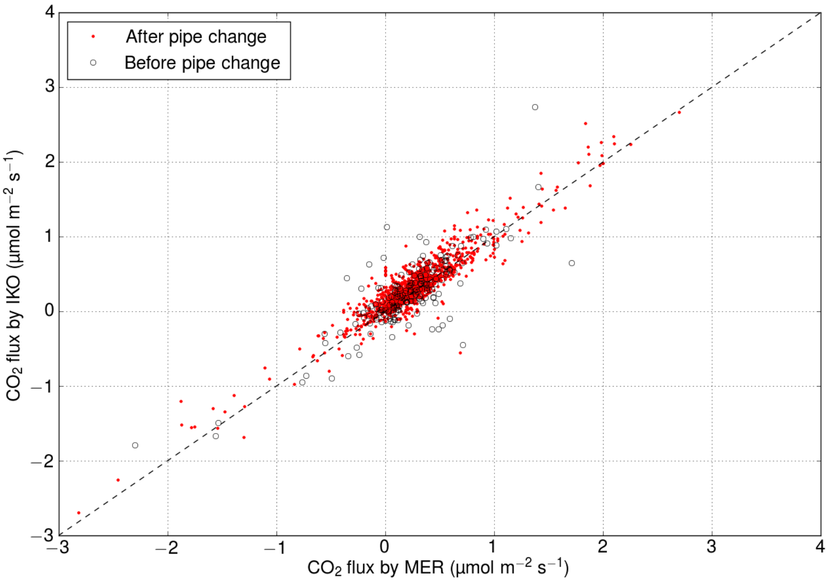

Figure 23: CO_2 flux by MER as a function of CO_2 flux by IKO. On 28 October 2016 pipelines were swapped: white circles represent the period when the IKO had virtual impactor equipped and red dots represent the period when the MER had the virtual impactor equipped.

air-sea fluxes of carbon dioxide (Fig. 23). Pearson product-moment correlation coefficient between the fluxes from the two closed-path instrument was 0.91. The mean difference between the CO_2 fluxes was $0.067\,\mu\mathrm{mol m^{-2} s^{-1}}$. However, since the most of the fluxes are small (94 % of all CO_2 fluxes are between -1 and $1\,\mu\mathrm{mol m^{-2} s^{-1}}$), the relative difference between the CO_2 fluxes measured with two instruments is large: mean absolute percentage error is 141 %. In contrast, the mean absolute percentage error of large values ($|F_{CO_2}| > 1\,\mu\mathrm{mol m^{-2} s^{-1}}$) is only 15 %. The measurements of small fluxes are obviously influenced by noise. The CO_2 fluctuations over sea are small compared to the instrument noise(Miller et al. 2010), which is a technical challenge. The correlation shows that the virtual impactor equipped to protect the instruments from the sea spray did not affect the fluxes.

4.4.2 Gas transfer velocity parametrization

There is a large difference between the measured CO_2 fluxes and the fluxes calculated with the parametrization of gas transfer velocity (Fig. 24). The Pearson product-moment correlation coefficient between MER and the parametrization is only 0.13. It appears that for small fluxes, the parametrization gives too low values. The high fluxes measured by the MER system are more in agreement with the parametrization.

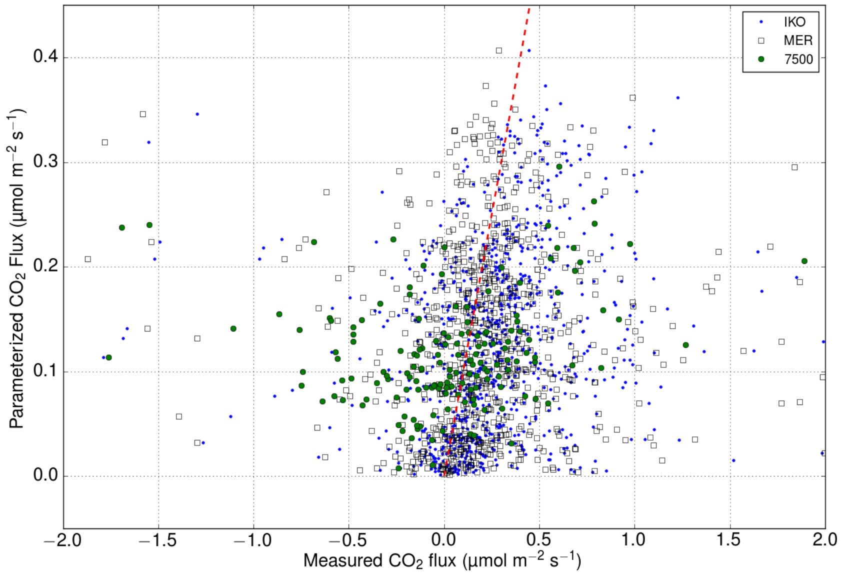

Figure 24: The modelled CO_2 flux as a function of measured flux. The red dashed line is 1:1 line.

As the seawater temperature dropped from 10.5 °C to 4.2 °C, the solubility of CO_2 increased from 50.8 $\mu mol m^{-3} atm^{-1}$ to 64.2 $\mu mol m^{-3} atm^{-1}$. Schmidt number increased at the same time from 1092 to 1621. These changes would cause a 3.7% increment in the flux. It should be remembered that seawater temperature, dissolved carbon dioxide and salinity are measured at the depth of 5 m. If the mixed layer is shallower than 5 m, our measurements do not represent the surface conditions. This would most likely be an issue with low wind speeds. The solar radiation, or even melting of sea-ice, can also affect by creating a stable surface layer. Temperature measurement can also be biased by the heat exchange between the sample water inside the pipe and water outside.

Atmospheric CO_2 concentration measured with Picarro can be regarded as a CO_2 concentration over the inlet since the spatial differences of CO_2 concentration in atmosphere are assumed to be small. Also, we have no reason to doubt the CO_2 measurements made with the carefully calibrated high-precision, laser-based Picarro instrument. The validation of SuperCO_2 data, however, has not been carried out yet.

The flux calculated with the eddy covariance method is the sum of all sinks and sources within the footprint area, which changes as a function of the wind direction, stability and other meteorological factors, whereas the wind speed-gas transfer -method depicts the flux in a predefined spot, i.e. the area above the inlet. However, the inlet is almost in the middle of the sea sector. Since we are dealing with coastal area, any heterogeneity in the fooptrint should be taken into consideration. There exists a few small islands in west-southwest from the flux tower, about 1.5 km away, which could cause a decrease in the flux measured with eddy covariance method.

4.4.3 Spectral analysis

The frequency response of the gas analyzers was examined by spectral analysis, as explained in Section 3.2.1. Due to the low magnitude of CO_2 fluxes over the sea, it was difficult to find situations in which the calculated cospectra were sufficiently smooth to facilitate a comparison with the correspondig Co_{wT}-cospectra. Most of the spectra examined, especially the ones for IKO and MER, were not well organized and were discarded. The fluctuations could be too small resulting in covariances dominated by instrument noise. Since representative cospectra were found more often for LI-7500 than for closed-path instruments, one can conclude that the tubing has an effect on the measurement spectrum. The flow most likely was not severely distorted since the temperature cospec-

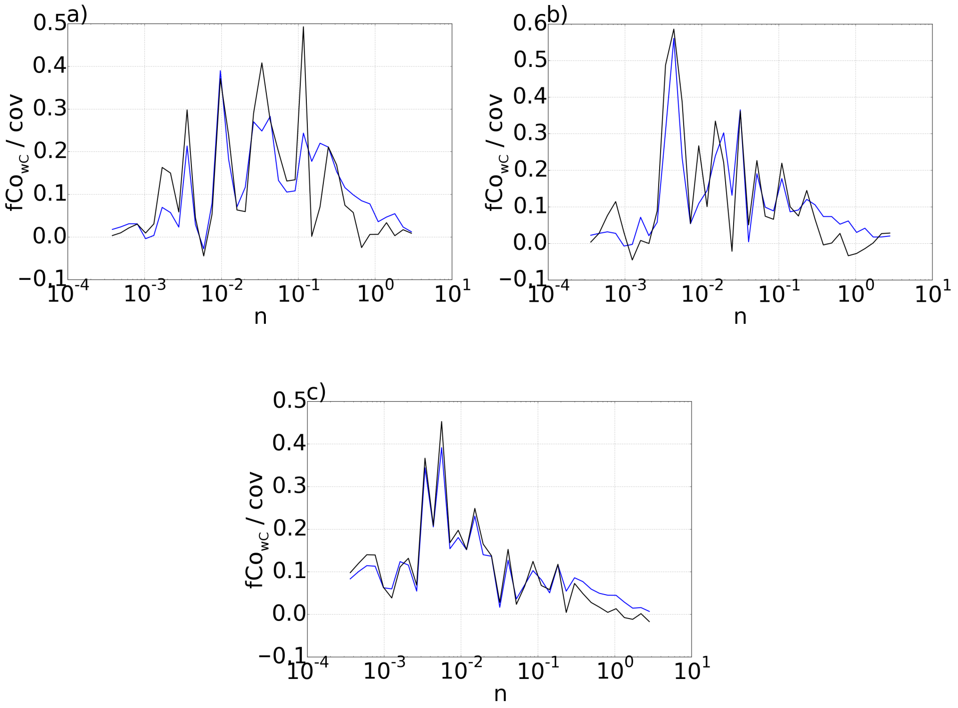

Figure 25: The Co_{wT} (blue line) and Co_{wC} (black line) of a) Licor LI-7000 IKO during 20 October 2016 12:00–12:30 UTC, b) Licor LI-7000 MER during 17 October 2016 11:00–11:30 UTC and c) Licor LI-7500 during 17 October 2016 13:30–14:00 UTC.

tra were well organized.

Examples of calculated cospectra indicate that cospectrum of the open-path follows closely the temperature cospectrum(Fig. 25). MER and 7500 both have maximum energy contribution at low frequencies, $0.001 < n < 0.01$, whereas IKO has high spikes also in higher frequencies. Cospectrum of MER has some difference at medium frequencies compared to the temperature cospectrum.

The half-power frequencies defined in Eq. (12) for IKO and MER were 0.66 Hz and 0.55 Hz respectively (Fig. 26). Some frequency loss was expected as the tubings are rather long and the flows are small. However, these results do not show that virtual impactor equipped to protect the instrument from sea spray has a significant effect on the high

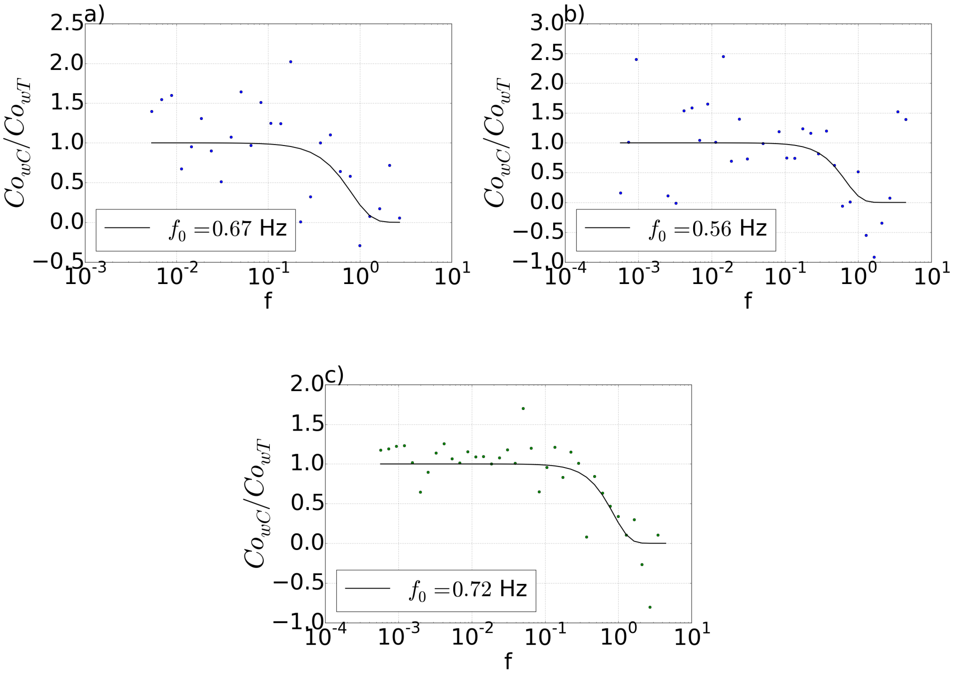

Figure 26: The ratio of Co_{wC} to Co_{wT} as a function of frequency and the gaussian fit of a) Licor LI-7000 IKO during 20 October 2016 12:00–12:30 UTC, b) Licor LI-7000 MER during 17 October 2016 11:00–11:30 UTC and c) Licor LI-7500 during 17 October 2016 13:30–14:00 UTC.

frequency range.

The half-power frequency for 7500 was largest, 0.73 Hz, meaning that the loss of high frequencies are smallest. However, a better response could be achieved by reducing the separation between the the LI-7500 and the anemometer, which in the present setup was 0.5 m(Fig. 11).

5 Conclusions

The recently established Atmospheric and marine research station measures a broad spectrum of physical, chemical and biological variables on an island in the Archipelago Sea. The station is equipped with a micrometeorological tower to measure air-sea fluxes of CO_2. A flow-through pumping system is used for monitoring dissolved CO_2 and pH.

The micrometeorological tower erected on the shore can be applied for measuring the air-sea fluxes of CO_2 in a certain wind sector. The sector was determined by examining the surface roughness length as a function of wind direction. Within the open sea sector, the mean surface roughness length was 1 mm, whereas outside this sector, the length was 12 cm. The air-sea fluxes of CO_2 measured during the study period 14 October - 14 December 2016 were mostly physically reasonable: the partial pressure difference between the sea and the air made the sea act as a source of CO_2.

The closed-path infrared gas analyzer employed at the site (Licor LI-7000) works well in the hard coastal conditions, while an open-path analyzer (Licor LI-7500) proved problematic due to its sensitivity to precipitation and high relative humidity. The fluxes measured with two different LI-7000 instruments were in good agreement, with a correlation coefficient of 0.91. The virtual impactor equipped on the pipeline of LI-7000 to protect the instrument from sea spray did not influence the CO_2 fluxes. Spectral analysis revealed that the open-path gas analyzer is the least affected by high frequency energy loss.

LI-7000 was found to be sensitive to changes in the instrument temperature. The dependence of the instrument temperature on CO_2 molar fraction of two LI-7000-instruments were $0.25\,\mathrm{ppm}\,°\mathrm{C}^{-1}$ and $0.18\,\mathrm{ppm}\,°\mathrm{C}^{-1}$. Due to this, it is advisable to place the instrument in a space where the changes in ambient temperature are minimal. This work led to development of the insulation of the instruments and more stable heating of the instrument shed.

CO_2 flux calculated using a parametrization of gas transfer velocity showed only a small correlation with the measured fluxes as the correlation coefficient was 0.13. The partial pressure difference between the sea and the air was small during the period, resulting in small measured fluxes, that may be dominated by noise. The comparison should be carried out during late summer, when the partial pressure difference is larger.

The flow-through pumping system was shown to be able to measure the aquatic inorganic carbonate system. The measured pH and dissolved CO_2 during July-October 2016 were closely linked to each other.

Acknowledgements

The Finnish Meteorological Institute has provided financial support for this thesis. I would like to thank my supervisors, Lauri Laakso and Juha-Pekka Tuovinen, for excellent guidance. Juha-Pekka Tuovinen proofread the thesis and provided corrections for grammar, notations and science. Thanks are also due to Sami Kielosto and Timo Mäkelä, who have taught me technical aspects of the measurements. I have learnt a lot during the time I have worked for FMI. I have been able to work independently, but at the same time I have been given the tools and support I need. It has been a pleasure to work in beautiful Utö. I am also grateful to my family and friends for the support.

References

Arya, S. P. (2001). *Introduction to micrometeorology.* 2nd ed. Orlando, Florida: Academic press, A Harcourt Science and Technology company.

Aubinet, M., C. Feigenwinter, B. Heinesch, Q. Laffineur, D. Papale, M. Reichstein, J. Rinne, and E. van Gorsel (2012). Nighttime flux correction. *Eddy covariance - A practical guide to measurement and data analysis.* Ed. by M. Aubinet, T. Vesala, and D. Papale. Dordrecht: Springer. Chap. 5, pp. 133–157.

Beer, S., M. Bjork, and J. Beardall (2014). *Photosynthesis in the Marine Environment.* 1st ed. Ames, Iowa: Wiley-Blackwell.

Blomquist, B., B. J. Huebert, C. Fairall, L. Bariteau, J. Edson, J. Hare, and W. McGillis (2014). Advances in Air-Sea CO_2 Flux Measurement by Eddy Correlation. *Boundary-Layer Meteorology* 152.

Burba, G. and D. Anderson (2010). *A brief practical guide to eddy covariance flux measurements.* 1.01. Lincoln, Nebraska: LI-COR, Inc.

LI-COR (2002). *LI-7500 CO2/H2O Analyzer - Instruction manual.* 2nd ed.

— (2005). *LI-7000 CO2/H2O Analyzer - Instruction manual.* 3rd ed.

Csanady, G. (2001). *Air-sea interaction, laws and mechanisms.* 1st ed. Cambridge: Cambridge University Press.

Etheridge, D., L. Steele, R. Langenfelds, R. Francey, J.-M. Barnola, and V. Morgan (1996). Natural and anthropogenic changes in atmospheric CO_2 over the last 1000 years from air in Antarctic ice and firn. *Journal Of Geophysical Research* 101.

Falkowski, P., R. J. Scholes, E. Boyle, D. Canadell J. Canfield, J. Elser, N. Gruber, K. Hibbard, P. Hogberg, S. Linder, F. T. Mackenzie, I. Moore B., T. Pedersen, Y. Rosenthal, S. Seitzinger, V. Smetacek, and W. Steffen (2000). The global carbon cycle: A test of our knowledge of Earth as a system. *Science* 290.

Feely, R., S. Doney, and S. Cooley (2009). Ocean Acidification: Present Conditions and Future Changes in a High-CO_2 World. *Oceanography* 22.

Finnish Meteorological Institute (2015). *Utö observations.* URL: `http://en.ilmatieteenlaitos.fi/uto-observations` (visited on 04/20/2017).

— (2017). *GHG Measurement sites.* URL: `http://en.ilmatieteenlaitos.fi/GHG-measurement-sites` (visited on 04/20/2017).

Foken, T., M. Aubinet, and R. Leuning (2012a). The eddy covariance method. *Eddy covariance - A practical guide to measurement and data analysis.* Ed. by M. Aubinet, T. Vesala, and D. Papale. Dordrecht: Springer. Chap. 1, pp. 1–19.

Foken, T., R. Leuning, S. Oncley, M. Mauder, and M. Aubinet (2012b). Corrections and data quality control. *Eddy covariance - A practical guide to measurement and data analysis.* Ed. by M. Aubinet, T. Vesala, and D. Papale. Dordrecht: Springer. Chap. 4, pp. 85–131.

Garbe, C. S., A. Rutgersson, J. Boutin, G. de Leeuw, B. Delille, C. W. Fairall, N. Gruber, J. Hare, D. T. Ho, M. T. Johnson, P. D. Nightingale, H. Pettersson, J. Piskozub, E. Sahlée, W. Tsai, B. Ward, D. K. Woolf, and C. J. Zappa (2014). Transfer Across the Air-Sea Interface. *Ocean-Atmosphere Interactions of Gases and Particles.* Ed. by P. S. Liss and M. T. Johnson. Springer Berlin Heidelberg, pp. 55–112.

Heinze, C., S. Meyer, N. Goris, L. Anderson, R. R. Steinfeldt, N. Chang, C. Le Quéré, and D. Bakker (2015). The ocean carbon sink – impacts, vulnerabilities and challenges. *Earth System Dynamics* 6.

Högström, U., E. Sahlée, W. Drennan, K. Kahma, A.-S. Smedman, C. Johansson, H. Pettersson, A. Rutgersson, L. Tuomi, and F. Zhang (2008). Momentum fluxes and wind gradients in the marine boundary layer - a multi-platfrom study. *Boreal Environment Research* 13.

Jacob, D. (1999). *Introduction to atmospheric chemistry.* 1st ed. Princeton, New Jersey: Princeton University Press.

Kagan, B. (1995). *Ocean-atmosphere interaction and climate modelling.* 1st ed. Cambridge: Cambridge University Press.

Kaimal, J. and J. Finnigan (1994). *Atmospheric boundary layer flows: their structure and measurement.* 1st ed. New York: Oxford University press, Inc.

Kulinski, K. and J. Pempkowiak (2011). The carbon budget of the Baltic sea. *Biogeosciences* 8.

Laakso, L. (2017). Unpublished. Personal communication. Accessed 20.1.2017.

Löffler, A., B. Schneider, M. Perttilä, and G. Rehder (2011). Air-sea CO_2 exchange in the Gulf of Bothnia, Baltic sea. *Continental Shelf Research* 37.

Miller, S. D., C. Marandino, and E. S. Saltzman (2010). Ship-based measurement of air-sea CO2 exchange by eddy covariance. *Journal of Geophysical Research: Atmospheres* 115.D2. D02304.

Millero, F. (1995). Thermodynamics of the carbon dioxide system in the oceans. *Geochmica et Cosmochimica Acta* 59.4.

Munger, J. W., H. W. Loescher, and H. Luo (2012). Measurement, tower, and site design considerations. *Eddy covariance - A practical guide to measurement and data analysis.* Ed. by M. Aubinet, T. Vesala, and D. Papale. Dordrecht: Springer. Chap. 2, pp. 21–58.

Myrberg, K., M. Leppäranta, and H. Kuosa (2006). *Itämeren fysiikka, tila ja tulevaisuus.* 1st ed. Helsinki: Yliopistopaino.

Norman, M. (2013). Air-Sea Fluxes of CO_2: Analysis Methods and Impact on Carbon Budget. PhD thesis. Uppsala University.

Norman, M., A. Rutgersson, L. Sorenson, and E. Sahlee (2011). Methods for estimating air-sea fluxes of CO_2 using high-frequency measurements. *Boundary-Layer Meteorology* 144.

Omstedt, A., M. Edman, L. G. Anderson, and H. Laudon (2010). Factors influencing the acid–base (pH) balance in the Baltic Sea: a sensitivity analysis. *Tellus B* 62.4.

Omstedt, A., M. Edman, B. Claremar, P. Frodin, E. Gustafsson, C. Humborg, H. Hägg, M. M., A. Rutgersson, G. Schurgers, B. Smith, T. Wällstedt, and A. Yurova (2012). Future changes in the Baltic Sea acid-base (pH) and oxygen balances. eng. Tellus, Series B: Chemical and Physical Meteorology. 64.

Omstedt, A., E. Gustafsson, and K. Wesslander (2009). Modelling the uptake and release of carbon dioxide in the Baltic Sea surface water. *Continental Shelf Research* 29.

Pirinen, P., H. Simola, J. Aalto, J.-P. Kaukoranta, P. Karlsson, and R. Ruuhela (2012). *Tilastoja Suomen ilmastosta 1981-2010.*

Rannik, U., A. Sogachev, T. Foken, M. Göckede, N. Kljun, and T. Leclerc M.Y. Vesala (2012). Footprint analysis. *Eddy covariance - A practical guide to measurement and data analysis.* Ed. by M. Aubinet, T. Vesala, and D. Papale. Dordrecht: Springer. Chap. 8, pp. 211–261.

Rutgersson, A., M. Norman, and G. Åström (2009). Atmospheric CO_2 variation over the Baltic sea and the impact on air–sea exchange. *Boreal Environment Research* 14.

Stewart, R. (1997). *Introduction to physical oceanography.* 1st ed. College Station, Texas: Texas A & M University.

Thomas, H. and B. Schneider (1999). The seasonal cycle of carbon dioxide in Baltic Sea surface waters. *Journal Of Marine Systems* 22.1.

Wanninkhof, R. (1992). Relationship between wind speed and gas exchange over the ocean. *Journal Of Geophysical Research* 97.

Wanninkhof, R., W. Asher, D. Ho, C. Sweeney, and W. McGillis (2009). Advances in quantifying air-sea exchange and environmental forcing. *Annual Review Of Marine Science* 1.

Weiss, R. F. (1974). Carbon dioxide in water and seawater: the solubility of a non-ideal gas. *Marine Chemistry* 2.

Wesslander, K. (2011). The carbon dioxide system in the Baltic Sea surface waters. PhD thesis. University of Gothenburg.